Brain intratumoural astatine-211 radiotherapy targeting syndecan-1 leads to durable glioblastoma remission and immune memory in female mice

Loris Roncali, Séverine Marionneau-Lambot, Charlotte Roy, Romain Eychenne, Sébastien Gouard, Sylvie Avril, Nicolas Chouin, Jérémie Riou, Mathilde Allard, Audrey Rousseau, et al.

Brain intratumoural astatine-211 radiotherapy targeting syndecan-1 leads to durable glioblastoma remission and immune memory in female mice

Loris Roncali,[a,b] Séverine Marionneau-Lambot,[b,c,d] Charlotte Roy,[a,e] Romain Eychenne,[b,f] Sébastien Gouard,[b,d] Sylvie Avril,[a] Nicolas Chouin,[b,g] Jérémie Riou,[h] Mathilde Allard,[b] Audrey Rousseau,[a,h] François Guérard,[b] François Hindré,[a,e] Michel Chérel,[b,d,i,k,*] and Emmanuel Garcion[a,e,j,k,**]

[a]Université d'Angers, INSERM, CNRS, CRCI²NA, F-49000, Angers, France
[b]Nantes Université, INSERM, CNRS, CRCI²NA, F-44000, Nantes, France
[c]CHU Nantes, Nantes Université, Service de médecine nucléaire, F-44000, Nantes, France
[d]CIMA (Centre d'Imagerie Multimodale Appliquée), Nantes Université, INSERM, CNRS, CRCI²NA, F-44000, Nantes, France
[e]PRIMEX (Plateforme de Radiobiologie et d'Imageries Expérimentales), Université d'Angers, SFR 4208, F-49000, Angers, France
[f]GIP ARRONAX, F-44160, Saint-Herblain, France
[g]ONIRIS, F-44000, Nantes, France
[h]CHU Angers, Université d'Angers, F-49000, Angers, France
[i]Institut de Cancérologie de l'Ouest, Service de médecine nucléaire, F-44160, Saint-Herblain, France
[j]PACEM (Plateforme d'Analyse Cellulaire et Moléculaire), Université d'Angers, SFR 4208, F-49000, Angers, France

eBioMedicine
2024;105: 105202
Published Online 20 June 2024
https://doi.org/10.1016/j.ebiom.2024.105202

Summary

Background Glioblastoma (GB), the most aggressive brain cancer, remains a critical clinical challenge due to its resistance to conventional treatments. Here, we introduce a locoregional targeted-α-therapy (TAT) with the rat monoclonal antibody 9E7.4 targeting murine syndecan-1 (SDC1) coupled to the α-emitter radionuclide astatine-211 (^{211}At-9E7.4).

Methods We orthotopically transplanted 50,000 GL261 cells of murine GB into the right striatum of syngeneic female C57BL/6JRj mice using stereotaxis. After MRI validation of tumour presence at day 11, TAT was injected at the same coordinates. Biodistribution, efficacy, toxicity, local and systemic responses were assessed following application of this protocol. The 9E7.4 monoclonal antibody was labelled with iodine-125 (^{125}I) for biodistribution and with astatine-211 (^{211}At) for the other experiments.

Findings The ^{211}At-9E7.4 TAT demonstrated robust efficacy in reducing orthotopic tumours and achieved improved survival rates in the C57BL/6JRj model, reaching up to 70% with a minimal activity of 100 kBq. Targeting SDC1 ensured the cerebral retention of ^{211}At over an optimal time window, enabling low-activity administration with a minimal toxicity profile. Moreover, TAT substantially reduced the occurrence of secondary tumours and provided resistance to new tumour development after contralateral rechallenge, mediated through the activation of central and effector memory T cells.

Interpretation The locoregional ^{211}At-9E7.4 TAT stands as one of the most efficient TAT across all preclinical GB models. This study validates SDC1 as a pertinent therapeutic target for GB and underscores ^{211}At-9E7.4 TAT as a promising advancement to improve the treatment and quality of life for patients with GB.

Funding This work was funded by the French National Agency for Research (ANR) "France 2030 Investment Plan" Labex Iron [ANR-11-LABX-18-01], The SIRIC ILIAD [INCa-DGOS-INSERM-18011], the French program "Infrastructure d'Avenir en Biologie-Santé" (France Life Imaging) [ANR-11-INBS-0006], the PIA3 of the ANR, integrated to the "France 2030 Investment Plan" [ANR-21-RHUS-0012], and support from Inviscan SAS (Strasbourg, France). It was also related to: the ANR under the frame of EuroNanoMed III (project GLIOSILK) [ANR-19-ENM3-0003-01]; the "Région Pays-de-la-Loire" under the frame of the Target'In project; the "Ligue Nationale contre le Cancer" and the "Comité Départemental de Maine-et-Loire de la Ligue contre le Cancer" (CD49) under the frame of the FusTarG project and the "Tumour targeting, imaging and radio-therapies network" of the "Cancéropôle Grand-Ouest" (France). This work was also funded by the Institut National de la Santé et de la Recherche Médicale (INSERM), the University of Nantes, and the University of Angers.

*Corresponding author. Université d'Angers, INSERM, CNRS, CRCI²NA, F-49000, Angers, France.
**Corresponding author. Nantes Université, INSERM, CNRS, CRCI²NA, F-44000, Nantes, France.
E-mail addresses: emmanuel.garcion@univ-angers.fr (E. Garcion), michel.cherel@univ-nantes.fr (M. Chérel).
[k]These authors contributed equally.

Keywords: Glioblastoma; Targeted-α-therapy; Astatine-211; Monoclonal antibody; Syndecan-1

Research in context

Evidence before this study

Glioblastoma (GB) is the most aggressive malignancy of the central nervous system. Since 2005, the standard treatment protocol consists of a surgical resection followed by radiotherapy and chemotherapy, but does not allow to surpass a median survival of 15 months. Over the past two decades, alternative therapeutic strategies for GB have faced challenges due to its specific localisation and strong resistance to therapy. Recent progress in targeted radionuclide therapy, especially with α-emitting radionuclides, have unveiled potential avenues. Successful early 2000s clinical trials with β^- radionuclides led to approved treatments for non-Hodgkin lymphoma (Zevalin®, Bexxar®), neuroendocrine tumours (Lutathera®) and metastatic castration-resistant prostate cancer (mCRPC; Pluvicto®). However, targeted-α-therapy (TAT) has shown the superiority of α radionuclides in cytotoxicity towards tumour cells and preservation of healthy tissue. Several clinical trials validated these findings and resulted in the approval in 2013 of the radium-223 (^{223}Ra) dichloride (Xofigo®) for the treatment of mCRPC. Unfortunately, translating these advances into satisfactory outcomes for GB remains elusive. Despite the clinical validation of safety and feasibility of TAT in patients with GB by Zalutsky et al. in 2008, subsequent preclinical models failed to provide a curative effect. These therapeutic approaches exhibited a vast design heterogeneity, and were limited by the use of subcutaneous grafts of GB into murine models, which poorly replicate the tumour microenvironment compared to orthotopic tumours.

Added value of this study

Our study investigates the application of a locoregional TAT in an orthotopic, syngeneic mouse model of GB, introducing the combination of the α radionuclide astatine-211 (^{211}At) and a rat monoclonal antibody targeting the GB biomarker syndecan-1. We aimed to evaluate the efficacy of TAT on an unresected and untreated orthotopic GB mouse model, leveraging the tumour presence to enhance TAT retention and reach infiltrative cells. In 2010, Cordier et al. demonstrated TAT feasibility and safety as a first-line protocol in a pilot study with five patients with GB. In our study, locoregional TAT demonstrated a strong efficacy, achieving a 70% survival rate with a minimal activity of 100 kBq. This optimal radionuclide-vector-biological target combination enabled low treatment activities, and demonstrated the establishment of immune memory responses in long-term survivors upon tumoural rechallenge.

Implications of all the available evidence

This study highlights the relevance of locoregional TAT for unresected and untreated GBs. Using a monoclonal antibody as a vector ensures an optimal local radioactivity retention, minimising systemic distribution upon elimination. The memory immunity induced in long-term survivors treated with TAT suggests the exploration of therapeutic combinations, particularly with immunotherapy, to maximise these effects. As Le Reste et al. indicated in 2021 a 60-day median survival with the conventional treatment protocol in the same murine model, our findings underscore the added value of TAT in the GB therapeutic arsenal. Furthermore, exploring its integration into the standard protocol could help to determine the optimal administration time window. These outcomes support considering a humanised anti-SDC1 antibody in future TAT investigations for GB, aiming for improved clinical outcomes in the coming years.

Introduction

Glioblastoma (GB) is the most aggressive form of brain cancer. Classified as a grade 4 astrocytoma by the World Health Organisation,[1] its annual incidence is 3.27 cases per 100,000 people.[2] Treatment typically involves a maximum safe resection, when feasible, followed by the application of the Stupp regimen - a conventional protocol which comprises external radiotherapy and concomitant temozolomide chemotherapy. Despite this intensive therapeutic approach, the median overall survival does not exceed 15 months,[3] primarily due to the radioresistance[4] and chemoresistance[5] of the remaining GB cells after surgical resection. Another key obstacle to therapeutic success is the blood–brain barrier (BBB), which shields the brain from systemic circulation and consequently hampers the intravenous administration of therapeutic agents.[6]

As phase III clinical trials have culminated in failures over the past 20 years to validate new GB therapies,[7] locoregional vectorised radiotherapy represents a promising approach to overcome these constraints and improve tumour targeting. Initially, β^--emitting radionuclides were investigated due to their optimal range in tissues (1–2 mm), high energy emission (0.1–2.3 MeV), and low linear energy transfer (LET; 0.2 keV/μm). In this context, our previous work demonstrated the extension of survival of GB-bearing rodents following the injection of lipid nanocapsules loaded with rhenium-188 (^{188}Re).[8–10]

In the past two decades, α emitters have demonstrated significant advantages over β^- emitters: a shorter range in tissues (50–100 μm), higher energy emission (2–10 MeV), higher LET (approximately 100 keV/μm),[11] and better efficacy in hypoxic conditions.[12] These characteristics make them particularly effective in eliminating tumours burdens and isolated tumour cells while minimising toxicity to healthy tissues. Thus, locoregional application of astatine-211 (^{211}At) prolonged survival in murine models of neoplastic meningitis[13] and ovarian cancer.[14] Treatment of brain metastasis has also been investigated with promising results.[15] Regarding GB, clinical trials and pilot studies have demonstrated the feasibility and low toxicity of intracranial administration of targeted-α-therapies (TATs) in patients, such as tenascin-targeted monoclonal antibodies (mAb) labelled with ^{211}At,[16] and substance P labelled with bismuth-213 (^{213}Bi)[17,18] or with actinium-225 (^{225}Ac).[19]

Among α emitters, ^{211}At has experienced an increasing worldwide supply, coupled with advancements in its chemistry, making it a prime candidate to develop TATs.[20,21] Based on a branching decay, ^{211}At generates one α particle of 5.9 MeV or 7.5 MeV with a LET of 99 keV/μm. Its half-life of 7.21 h is convenient for multistep-radiolabelling and is suitable for injection to patients. Recent preclinical studies have demonstrated the ability of ^{211}At to reduce tumour growth using various vectorisation approaches, such as peptides and gold nanoparticles, through intravenous,[22–24] intraperitoneal,[25] or intratumoural administration.[26–28] While some significant improvements in survival were observed,[22,24,28] no curative effect was found. These studies were primarily conducted on subcutaneous rodent models of GB, and no locoregional TAT administration in orthotopic GB models have been investigated yet.

In this context, we aimed to develop a locoregional therapy to target tumour burdens and disseminated cells. MAbs represent ideal vectors for locoregional TAT due to their high affinity and specificity for their target and extensive biological half-life. In this study, we selected the 9E7.4 rat mAb directed against the murine cell surface proteoglycan syndecan-1 (SDC1, also known as CD138) to target GB. We previously demonstrated that the labelling of the 9E7.4 mAb with ^{211}At resulted in efficient systemic targeting and elimination of disseminated cells in a multiple myeloma model, without altering its specific binding to SDC1.[29] In GB, the overexpression of SDC1 is associated with a poor prognosis. It establishes a critical interface between tumour cells and their microenvironment by engaging with the extracellular matrix and with numerous growth factors and cytokines,[30] thus influencing tumoural anchoring, invasion, immunosuppression, and radioresistance.[31–33] Targeting SDC1 could ensure extended retention of radioactivity and potentially enable the disruption of the entire tumour ecosystem.

In this study, we developed an orthotopic, syngeneic mouse model of GB to assess the efficacy of ^{211}At when coupled to the 9E7.4 mAb (^{211}At-9E7.4). The orthotopic approach would allow to recapitulate a GB microenvironement closer to reality, and the use of a syngeneic model could ensure the investigation of local and systemic immune responses. Therapeutic efficacy was assessed by magnetic resonance imaging (MRI) and toxicity through weekly blood sampling. Importantly, we carefully tracked tumour progression and the emergence of potential secondary tumours within the brain parenchyma, while measuring the effects of the TAT in the induction of potential antitumour immune responses.

Methods

Ethics

This project was conducted with the authorisation of the French Ministry of Higher Education and Research, in accordance with the stipulations of European Directive 2010/63/EU dated September 22, 2010. All surgical procedures were performed under ketamine/xylazine anesthesia and all measures were taken to minimise the discomfort and pain endured by the animals. The preclinical studies were conducted on the UTE platform (SFR François Bonamy, IRS-UN, University of Nantes, France - Authorisation D44-278). The authorisations concerning animal experimentation (APAFIS #22777, APAFIS #27292, APAFIS #34964) were delivered by the Ministry of Higher Education and Research, after a favorable review from the local animal experimentation ethics committee "Pays de la Loire (CEEA-06)".

Mice

152 Specific Pathogen Free (SPF) 7-weeks female C57BL/6JRj mice (RRID: MGI:2670020) were procured from Janvier Labs and used for experimentation one week after delivery. Female mice were chosen due to their reduced aggressive behavior during housing. Mice were accommodated in polycarbonate cages within a specific pathogen-free environment with regulated conditions including a temperature of 22 °C, humidity within the range of 50–70%, and a 12-h light/dark cycle. The room ambient air was frequently refreshed at a rate of 10 air changes per h (ACH). Mice were provided with *ad libitum* access to tap water and food. In this work, each mouse represents an independent experimental unit.

Cell line

The GL261 cell line (RRID: CVCL_Y003) was kindly provided by Corinne Griguer and G. Yancey Gillespie of the University of Alabama at Birmingham, AL, USA. GL261 cells were detached from culture dishes using accutase (A6964, Sigma–Aldrich) for 5 min at 37 °C, and then suspended in Dulbecco's Modified Eagle's Medium

(DMEM; D6429, Sigma–Aldrich) supplemented with 10% fetal bovine serum (FBS; CVFSVF00-01, Eurobio Scientific) and 1% antibiotic solution (A5955, Sigma–Aldrich). Cells were then centrifuged at 120×*g* and counted. Subsequently, the cells were cultured in a humidified incubator at 37°C, 5% CO_2, 21% O_2, and 100% humidity and used when 80–90% confluence was reached. The cell line was tested mycoplasma-negative with a HEK-blue detection kit (Invivogen).

9E7.4 mAb production

The 9E7.4 mAb was produced by immunisation of a rat with a 40-amino-acid peptide derived from the murine SDC1 protein (amino acid sequence 90–130, GenBank: CAA80254.1), which was procured from GeneCust. The isotype of the rat used in generating 9E7.4 was determined with a RMT1 Rat Isotyping Kit (Bio-Rad) in strict adherence to the protocol provided by the manufacturer. The specificity and affinity of 9E7.4 mAb towards SDC1 was previously demonstrated by flow cytometry.[29]

^{125}I or ^{211}At-labelling of 9E7.4 and IgG2a, κ mAb

[^{125}I]NaI was obtained commercially from PerkinElmer in 10^{-5} M NaOH solution with a volume activity of 3.70 MBq/μL. [^{211}At]NaAt was produced at the Arronax cyclotron facility (Saint-Herblain, France) using the ^{209}Bi(α,2n)^{211}At reaction and recovered from the irradiated target in chloroform using a dry distillation protocol adapted from the procedure previously reported by Lindegren et al.[34] [^{211}At]NaAt was then obtained by reducing to dryness the chloroformic astatine solution under a gentle stream of nitrogen to obtain dry astatine, followed by dissolution in an appropriate volume of 10 mg/mL dithiothreitol aqueous solution. The isotype control used for experiments was a rat IgG2a, κ purchased from R&D Systems. Radioiodination or astatination of 9E7.4 and IgG2a, κ mAb were performed using a two-step process, from a biaryliodonium salt precursor of *N*-succinimidyl-3-[^{125}I]-iodobenzoate ([^{125}I]SIB) or *N*-succinimidyl-3-[^{211}At]-astatobenzoate ([^{211}At]SAB) and adapted from a previous work.[35] 3-(succinimidyloxycarbonyl)phenyl(4-methoxyphenyl)iodonium triflate (for astatination) or 3-(succinimidyloxycarbonyl) phenyl(2-thienyl)iodonium triflate for radioiodination (2.5 mM in CH_3CN, 190 μL) was incubated with [^{125}I]NaI or [^{211}At]NaAt solution for 30 min at 100 °C and 60 °C respectively. The crude reaction solution was then deposited on a dry disposable Sep-Pak C_{18} Plus Long cartridge (Waters), washed with 45 mL of CH_3CN 20% in H_2O and 2 mL of CH_3CN 100% to dissolve the expected product. CH_3CN fraction was diluted with 10 mL of H_2O, concentrated on a Sep-Pak C_{18} Plus Light (Waters) and recovered with 600 μL of MeCN. After evaporation under a stream of nitrogen, the resulting dry [^{125}I]SIB or [^{211}At]SAB was dissolved in 10 μL DMSO, followed by the addition of 60 μL of either the 9E7.4 mAb or the isotype control IgG2a, κ (concentration of 5 mg/mL in 0.3M borate buffer at pH 8.6 using a disposable Amicon Ultra-4 centrifugal unit (Millipore)). The solution was incubated for 30 min at 20 °C, and conjugation yields were assessed by ITLC-SG analysis of a sample aliquot (methanol as eluent) and scanned with a Cyclone phosphor imaging scanner (PerkinElmer). Unbound [^{125}I]SIB or [^{211}At]SAB was removed using a NAP-5 size exclusion chromatography column (Sephadex G25, Cytiva) with saline solution (0.9% NaCl) as eluent. 200 μL fractions were collected and only the fraction with most activity was kept in order to isolate the highest volume activity. Ultimately, the radiochemical purity was evaluated by ITLC-SG analysis. For ^{125}I radioconjugates, volumic activity was 6 kBq/μL and activity concentration was 10.7 kBq/μg of mAb at the start of the *in vivo* injections. For ^{211}At radioconjugates, volumic activities and activity concentrations at the start of the *in vivo* injections are available in Table S1. The ^{211}At-labelling experiments were performed using five distinct ^{211}At productions.

Orthotopic tumour grafts

GL261 cells were detached with accutase (A6964, Sigma–Aldrich), counted and measured for viability by eosin exclusion. Animals were anaesthetised intraperitoneally with ketamine 0.8 mL/kg (Imalgene 1000, Mérial) and xylazine 0.62 mL/kg (Rompun 2%, Bayer). The mouse skull was pierced with a burr (Microtorque II) following these coordinates from the bregma (=0 mm): lateral: −2.1 mm, anteroposterior: +0.5 mm, depth: −3 mm. C57BL/6JRj mice received a tumour graft of 50,000 GL261 cells in the right striatum using a stereotaxis frame (Stoelting) with a 32G syringe (1702N, Hamilton Company) in a 5 μL volume of DMEM medium (D6429, Sigma–Aldrich) without FBS nor antibiotic. For the rechallenge grafts, 50,000 GL261 cells were injected at d162 into the left striatum with the same procedure at the following coordinates from the bregma (=0 mm): lateral: +2.1 mm, anteroposterior: +0.5 mm, depth: −3 mm. In both survival and rechallenge studies, the presence of the tumour in the striatum was validated by day 11 (d11) by a T2 hypersignal on MRI. Absence of tumour detection by d11 was *a priori* established as an exclusion criterion. The tumoural model achieved a tumour engraftment rate of 89.5% with 16 out of 152 mice excluded from the study.

MRI

Mice from the survival and rechallenge studies were monitored with MRI. For each MRI procedure, mice were anaesthetised with 5% isoflurane and maintained at 2% isoflurane. MRI follow-up was conducted using a 3T magnetic field RS^{2}D device to assess tumour development and detect potential oedema/necrotic areas. Two types of sequences were employed to obtain axial sections. T2-weighted parameters were: field of view (FOV): 78 mm/32 mm/27.9 mm, echo time (TE): 64.48 ms, repetition time (TR): 5000 ms, flip angle: 90°,

acquisition matrix: 450/144/31/1, acquisition voxel size: 173.4 μm/177.8 μm/800 μm, bandwidth: 110.1 kHz, duration: 6 min 10 s. T1-weighted parameters were: FOV: 80 mm/40 mm/31 mm, TE: 12,07 ms, TR: 769 ms, flip angle: 90°, acquisition matrix: 450/144/31/1, acquisition voxel size: 178.8 μm/277.8 μm/800 μm, bandwidth: 50.09 kHz, duration: 9 min 21 s. Due to a technical maintenance issue with the RS^2D device, the group treated with unlabeled 9E7.4 mAb in the survival study was imaged with a Bruker Biospec 70/20 device equipped with a 1H cryoprobe and which operates at a magnetic field of 7T (Bruker). T2-weighted sequence: FOV: 2 cm × 2 cm, TE: 14 ms, TR: 2000 ms, acquisition matrix: 256 × 256, slice thickness: 0.5 mm (separated from 0.1 mm), 2 averages, rare factor = 4, fat saturation. T1-weighted sequence: FOV: 2 cm × 2 cm, TE: 2.6 ms, TR: 2000 ms, acquisition matrix: 256 × 256, slice thickness: 0.5 mm (separated from 0.1 mm), 2 averages, flip angle = 80°, fat saturation. Images were analysed using the OsiriX MD software (v11.0).

Radioconjugates locoregional injection

Radioconjugates were locally administered 11 days after the GL261 cells inoculation. To achieve an adapted distribution volume from a 5 μL injection volume, radioconjugates were injected by convection-enhanced delivery (CED), allowing the safe and homogeneous distribution of highly concentrated agents independently of their molecular weight or diffusivity.[36,37] The radioconjugates and their controls were injected into the striatum at the same coordinates as the tumour graft, using a stereotaxic frame (Stoelting) equipped with a 32G syringe (1702N, Hamilton Company) connected to a convective infusion pump (Pump 11 Elite, Harvard Apparatus) delivering at a rate of 1 μL/min. The ^{125}I-labeled conjugates were prepared to obtain 2.8 μg of labeled antibodies (9E7.4 mAb or IgG2a, κ) with 30 kBq of ^{125}I in a volume of 5 μL of saline solution (0.9% NaCl). ^{211}At-labeled conjugates were injected at three different activities (470, 200 and 100 kBq) in a single injection of 5 μL. The ^{211}At-labeled conjugates were prepared to obtain 2.8 μg of labeled antibodies (9E7.4 mAb or IgG2a, κ) with 470 kBq of ^{211}At in a volume of 5 μL of saline solution (0.9% NaCl). Taking into account the decay of ^{211}At, dilutions were performed to obtain the other activities: 200 kBq with 1.12 μg of antibody, and 100 kBq with 0.56 μg of antibody, in 5 μL of saline solution (0.9% NaCl). All untreated mice received an injection of 5 μL of saline solution (0.9% NaCl) under the same conditions.

Biodistribution

C57BL/6JRj mice received a tumour graft of 50,000 GL261 cells in the right striatum (n = 24). At d11, mice were randomly allocated to groups before a striatal injection of 30 kBq of ^{125}I-9E7.4 (n = 12) or IgG2a, κ (n = 12). Blood, thyroid, skin, muscle, spleen, stomach, small intestine, kidneys, liver, heart, lungs, salivary glands, and brain were collected and weighed (except for the thyroid due to difficulty in sampling alone) at 2 h, 7 h, 21 h, and 72 h after injection (n = 3 for each group). The radioactivity was then counted for each sample with a Hidex automatic gamma counter (calibrated and normalised). The measured radioactivity values were decay-corrected to be normalised over the given sacrifice time.

Dosimetry

Dosimetry was conducted based on results from *ex vivo* biodistribution studies. Time–activity curves for each organ/tissue were fitted using a single exponential function or a sum of two exponentials. Cumulated activities in each organ/tissue were determined by integrating these single or dual exponential functions from 0 to infinity. The time-integrated activity for each organ was then calculated by determining the area under each fitted time–activity curve. Finally, absorbed doses were calculated assuming local energy deposition within all organs: time-integrated activities, weighted by tissue mass, were multiplied by the energy of emitted α particles (6.79 MeV per decay), considering the contribution of ^{211}At and polonium-211 (^{211}Po) with the appropriate branching ratio, according to the MIRD radionuclide data and decay schemes.[38]

Digital autoradiography

C57BL/6JRj mice received a tumour graft of 50,000 GL261 cells in the right striatum (n = 9) and were randomly allocated to groups at d11. After the striatal CED injection of 30 kBq of ^{125}I-9E7.4 at d11, the brain was harvested after 2 h, 7 h, or 21 h post-injection, and quickly frozen in 2-methyl-butane at –25 °C for 1 min 30 s (n = 3 for each group). 10 μm coronal brain cryosections were obtained using a cryostat (CM3050S, Leica) and were placed on SuperFrost Plus slides (VWR). Digital autoradiography was performed using a BeaQuant digital autoradiography instrument with the Beavacq software (Ai4R) for an acquisition time of 8 h, following the supplier's instructions.

Survival and rechallenge studies

In the survival study, C57BL/6JRj mice received a tumour graft of 50,000 GL261 cells in the right striatum (n = 61). On d11, the presence of the tumour was validated by MRI. Allocation to groups was stratified based on tumor size. A CED injection of the ^{211}At-9E7.4 TAT or its corresponding control conditions was carried out at the same coordinates. In one experiment (n = 5), the 470 kBq group received 473.7 ± 17.7 kBq (2.8 μg of antibody). In three independent experiments (n = 16), the 200 kBq group received 206.4 ± 9.3 kBq (1.12 μg of antibody). In two independent experiments (n = 10), the 100 kBq group received 99.7 ± 9 kBq (0.56 μg of antibody). Additionally, five mice received 93.5 ± 3.5 kBq of ^{211}At-IgG2a, κ (0.56 μg of antibody), four mice received 98.2 ± 4.2 kBq of

[^{211}At]NaAt and six mice received 2.8 μg of unlabelled 9E7.4 mAb. The activities were obtained by diluting the stock solutions with saline solution (0.9% NaCl), taking into account the decay of ^{211}At. All untreated mice (n = 15) received an injection of 5 μL of saline solution (0.9% NaCl) under the same conditions. A retro-orbital blood sampling was conducted once a week to measure haematological toxicity using a haematology analyser (Element HT5, Scil). Once a month, a retro-orbital blood sample was taken to measure biochemical parameters (Element RC, Scil). For the rechallenge study, 15 out of the 17 long-surviving mice were administered a graft of 50,000 GL261 cells into the left striatum on d162 along (470 kBq: n = 3; 200 kBq: n = 6; 100 kBq: n = 6; control n = 12; total n = 27). Two long-survivors were excluded from the rechallenge study: One mouse died due to anesthesia before the graft, and one mouse died from an unknown cause on d13. In both survival and rechallenge studies, mice were weighed and monitored by MRI on a weekly basis and were euthanised upon weight loss exceeding 20% of initial weight, combined with the deterioration of general condition and the appearance of significant pain symptoms (reduced activity, reduced food and drink intake, orbital tightening, abnormal ear position, aggression and vocalisation).

Histopathological analysis

C57BL/6JRj mice received a tumour graft of 50,000 GL261 cells in the right striatum (n = 12) and were randomly allocated to groups at d11. After striatal injection of 200 kBq (n = 4) or 100 kBq (n = 4) of ^{211}At-9E7.4 mAb, or saline solution (0.9% NaCl; n = 4) at d11, mice were sacrificed at d18 and brains were harvested and quickly frozen in 2-methyl-butane at –25 °C for 1 min 30 s. 10 μm coronal brain cryosections were obtained using a cryostat (CM3050S, Leica) and were placed on SuperFrost Plus slides (VWR). They were stained with hematoxylin and eosin (HE) and scanned using a Nanozoomzer slide scanner (Hamamatsu). Histopathological analyses were carried out at the Department of Cellular and Tissue Pathology of the University Hospital Center of Angers (CHU-Angers, France). Images were analysed with the NPD view2 software (v2.9.29).

Immunofluorescence

C57BL/6JRj mice received a tumour graft of 50,000 GL261 cells in the right striatum (n = 8) and were randomly allocated to groups at d11. Following the injection of 200 kBq of ^{211}At-9E7.4 TAT (n = 4), or saline solution (0.9% NaCl; n = 4) into the striatum on d11, mice were sacrificed on d18. The brains were collected and rapidly frozen in 2-methyl-butane at –25 °C for 1 min 30 s, and then stored at –80 °C. Coronal brain cryosections of 10 μm thickness were obtained using a cryostat (CM3050S Leica) and placed on SuperFrost Plus slides (VWR). The sections were fixed with acetone for 10 s, rehydrated with PBS for 5 min, and then fixed with 4% paraformaldehyde (PFA) for 15 min at –20 °C. To minimise nonspecific binding, saturation with 10% normal goat serum (NGS) was conducted at room temperature (RT) for 45 min, followed by three PBS washes (5 min each). The sections were incubated overnight at 4 °C with primary antibodies diluted in PBS/Bovine Serum Albumin (BSA) 4% to a final concentration of 5 μg/mL. The primary mAbs used were anti-SDC1 (9E7.4), anti-CD31 (550274, BD Biosciences, RRID: AB_393571), anti-CD45 (14-0451-82, eBioscience, RRID: AB_467251), anti-CD11b (14-0112-82, eBioscience, RRID: AB_467108), anti-CD3 (14-0032-82, eBioscience, RRID: AB_467053), anti-CD4 (14-0041-82, eBioscience, RRID: AB_467063), anti-CD8 (14-0081-82, eBioscience, RRID: AB_467087) and control isotypes rat IgG2a, κ (553927, BD Pharmingen, RRID: AB_395142), and rat IgG2b, κ (559478, BD Pharmingen, RRID:AB_10056899). Following a PBS wash (3 × 5 min), biotinylated anti-rat (BP-9400, Vector Laboratories, RRID: AB_3073814), anti-rabbit (BA-1000, Vector Laboratories, RRID: AB_2313606), or anti-mouse (MKB-2225, Vector Laboratories, RRID: AB_2336564) IgG secondary antibodies (1:100) diluted in PBS/4% BSA were used for detection of the primary antibodies. After 1 h at RT, the sections were washed with PBS (3 × 5 min). Subsequently, the sections were developed using FITC-conjugated streptavidin (1:500, Dako) diluted in PBS for 45 min at RT, followed by a PBS wash (3 × 5 min). DAPI was added to the slides (1:1000) for 1 min, followed by another PBS wash (3 × 5 min). Finally, the slides were mounted using Dako Fluorescent Mounting Medium. The labelled cryosections were analysed under an epifluorescence microscope (Axioscope 2 MOT, Zeiss) equipped with a camera (Axiocam 305, Zeiss). Images were acquired using the ZEN Blue v3.2 software (Zeiss). Quantitative analysis was performed using the FIJI software (v2.9.0).

PET/CT

[^{18}F]fluorodeoxyglucose ([^{18}F]FDG) was provided by the Nuclear Medicine service of the University Hospital Center of Nantes, France. PET/CT acquisitions were obtained at d34 after the rechallenge graft using an Iris PET/CT scanner (Inviscan imaging system) following the injection into the caudal vein of 4.725 ± 0.05 MBq of [^{18}F]FDG in a volume of 100 μL (n = 3). For the control mouse (n = 1), two acquisition times were implemented, at 90 min and 285 min post-injection. For the long-surviving mice (^{211}At-9E7.4200 kBq n = 1; ^{211}At-9E7.4100 kBq n = 1), only one time point at 90 min post-injection was carried out. Images were reconstructed using the OsiriX MD software (v11.0).

Flow cytometry

For the validation of SDC1 expression in the GL261 cell line, cells were saturated in a PBS/BSA 5% solution for 30 min at 4 °C after a PBS/BSA 1% wash. They were

subsequently incubated with the primary antibody 9E7.4 or its isotype control rat IgG2a, κ (553927, BD Pharmingen, RRID: AB_395142) for 30 min at RT. The secondary antibody anti-rat IgG conjugated with Alexa Fluor 546 (A11081, Invitrogen, RRID: AB_141738), was added for a 30 min incubation at 4 °C, protected from light. After two washes with PBS/BSA 1%, the cells were resuspended in PBS for analysis on a CytoFLEX LX cytometer (Beckman Coulter). For post-rechallenge blood sample analysis, 100 µL of blood were sampled for each mouse into EDTA tubes (control group: $n = 6$, rechallenge group: $n = 5$). An erythrocytes lysis step was performed using a BD Pharm Lyse lysis buffer and cells were then incubated for 15 min at RT, protected from light. After a PBS/BSA 1% wash, cells were saturated in a PBS/BSA 5% solution complemented with Purified Rat Anti-Mouse CD16/CD32 (Mouse BD Fc Block, BD Biosciences) for 30 min at 4 °C. Cells were then incubated with coupled primary antibodies during 30 min at RT, protected from light: anti-CD45-VioGreen™ (130-110-803, Miltenyi, RRID: AB_2658224), anti-CD3-FITC (11-0031-82, eBioscience, RRID: AB_464882), anti-CD4-PE-Cy7 (552775, BD Pharmingen, RRID: AB_394461), anti-CD8-APC-eFluor™ 780 (47-0081-82, eBioscience, RRID: AB_1272185), anti-CD44-BV510 (563114, BD Horizon, RRID:AB_2738011), anti-CD62L-APC (553152, BD Pharmingen, RRID: AB_398533). The samples were analysed on an Attune NxT cytometer (Invitrogen). All cytometry data were processed using the FlowJo software (v10.8.2).

Statistical analysis

This study followed the ARRIVE guidelines (Animal Research: Reporting of In Vivo Experiments). Quantitative data are presented as mean ± *SD* for experiments that did not undergo statistical tests (biodistribution, weights, and data compared to toxicity thresholds), or as median with interquartile range (*IQR*) for experiments analysed with non-parametric tests. Tumor volume curves are displayed as individual values due to decreasing sample size over time. Normality was assessed using graphical analyses with density plots. Sample sizes were determined based on feasibility considerations as this is an exploratory study aimed at generating new hypotheses and identifying response trends not described in the literature. Comparisons between two groups were conducted using the Mann–Whitney test. Comparisons of repeated measures between multiple groups were performed using the Friedman test with *post hoc* Dunn correction for pairwise comparisons. Mice were randomly assigned to groups except for survival and rechallenge studies, where allocation to groups was stratified based on tumor size as it is a confounding factor for these analyses. Survival data were presented using Kaplan–Meier curves, and significance was assessed using the Log–Rank test. Hazard ratio (HR) and 95% confidence interval (95% CI) for each group were determined using Cox proportional hazard regression, considering weight as a covariate. All tests were two-tailed and considered significant when p-values were <0.05. Data analysis was performed using the GraphPad Prism software (v9.5.0).

Role of funders

The funders of the study had no role in study design, data collection, data analysis, data interpretation, writing of the manuscript, or the decision to submit it for publication.

Results

In vivo GL261 tumours as a relevant model to target SDC1 in GB

The interest in targeting SDC1 in GB arises primarily from its correlation with a poor prognosis in patients. Using the information provided by the TCGA_GBM RNA-seq dataset accessible *via* the GlioVis portal (gliovis.bioinfo.cnio.es) in patients with IDH wild type GB, we observed that $SDC1^{HIGH}$ GBs provide a significantly lower median overall survival (11 months) than $SDC1^{LOW}$ GBs (14.9 months) with $*p = 0.0247$ (Log–Rank test) and hazard ratio (HR) = 0.66 with 95% confidence interval (95% CI): 0.46–0.95 (Cox proportional hazards regression; Fig. 1a). We established a preclinical model using the murine GB cells GL261, which were stereotactically injected into immunocompetent C57BL/6JRj mice. We assessed the relevance of SDC1 targeting with the 9E7.4 mAb in our model by quantifying the level of *in vitro* expression of SDC1 by flow cytometry in the GL261 cell line ($n = 6$). The ratio of the median fluorescence intensity (MFI) between the 9E7.4 mAb and the IgG2a, κ isotype control was >3.19. As the MFI ratio >2, we estimated that SDC1 is expressed in a majority of the cell population (Fig. 1b, Table S2).

We assessed the expression of SDC1 by tumour cells *in vivo* in C57BL/6JRj mice that received a stereotactic intra-striatal graft of 50,000 GL261 cells ($n = 4$). Mice were sacrificed after a weight loss >20% at d32, d38, d38 and d44, respectively. The analysis of frozen brain sections by immunofluorescence showed SDC1 to be significantly expressed at higher levels in the developed tumour than in the healthy parenchyma with $*p = 0.028571$ (Fig. 1c and d). In our study, the ^{211}At-9E7.4 TAT was injected on d11 at the same stereotactic coordinates *via* CED after confirming tumour presence by MRI the same day. The global efficacy of the treatment was evaluated by weekly MRI and blood sampling (Fig. 1e). The ^{211}At-labelling experiments were performed using five distinct productions of ^{211}At characterised by a ^{210}At/^{211}At ratio comprised between $3.2.10^{-3}$ and 2.10^{-5} (0.002 ± 0.001). The resulting astatinated antibody was prepared with a radiochemical purity of 98 ± 1%, hence, above the minimum requirement of

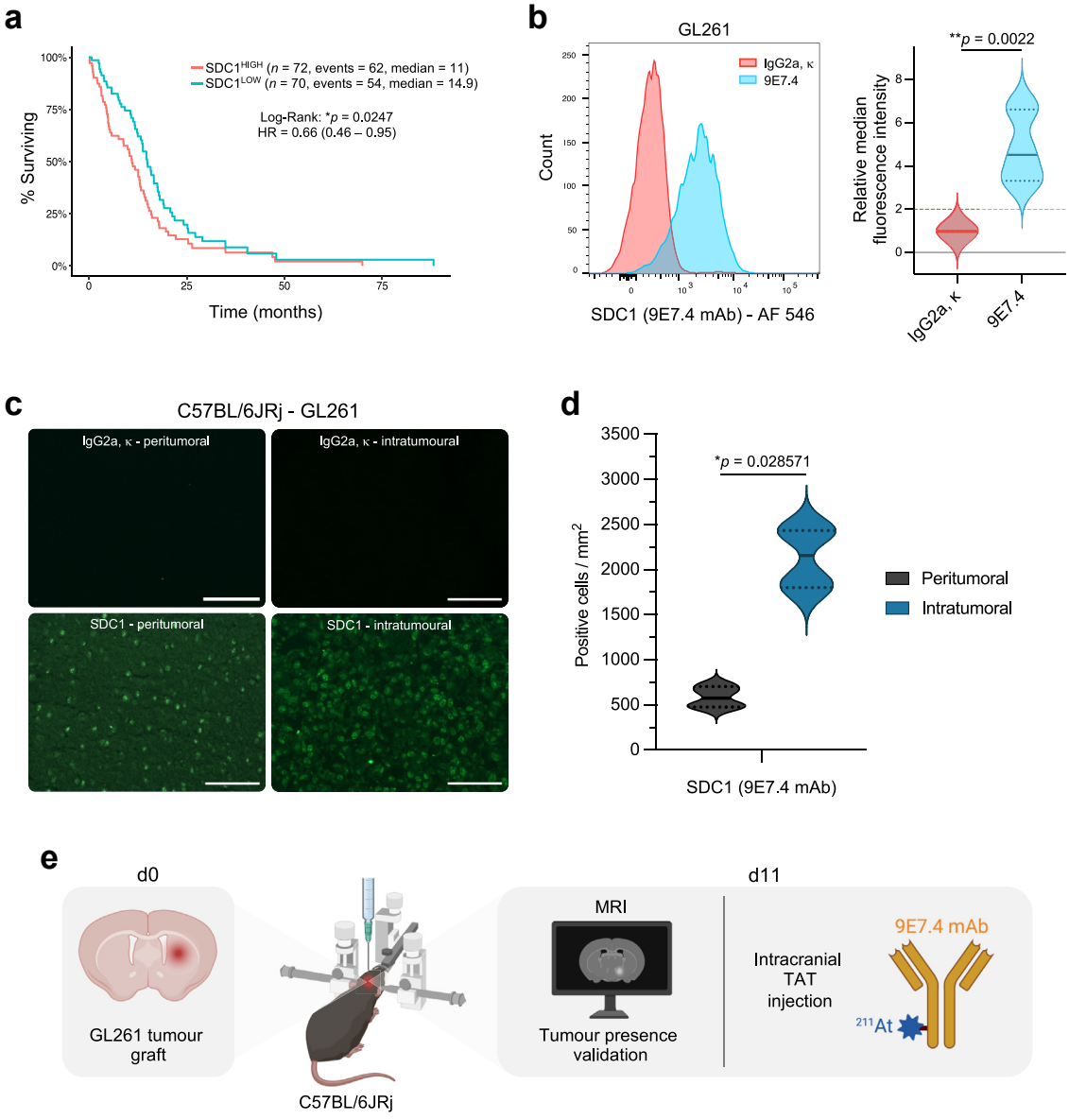

***Fig. 1:* In vivo GL261 tumours as a relevant model to target SDC1 in GB.** **(a)** Kaplan–Meier survival curves in patients with GB (IDH wild type) according to their level of SDC1 expression ($SDC1^{HIGH}$: $n = 72$, $SDC1^{LOW}$: $n = 70$). A Log–Rank test was performed to assess significance between the two groups. *$p < 0.05$. Hazard ratio and 95% confidence interval were determined using Cox proportional hazard regression. The GlioVis data portal was used for visualisation and analysis of SDC1 expression in patients with GB from the TCGA_GBM RNA-seq dataset (glio-vis.bioinfo.cnio.es). **(b)** Expression level of SDC1 in the murine GB cell line GL261 by flow cytometry ($n = 6$). SDC1 was detected with the 9E7.4 mAb as primary antibody. Data are presented as median with interquartile range (*IQR*). A Mann–Whitney test was used to assess significance between the two groups. **$p < 0.01$. **(c)** Immunofluorescence staining showing *in vivo* expression of SDC1 in orthotopic GL261 tumours. C57BL/6JRj mice were injected with 50,000 GL261 cells and sacrificed after a weight loss >20%. SDC1 was detected with the 9E7.4 mAb as primary antibody. Scale bar = 100 µm ($n = 4$). **(d)** SDC1 positive cells counting in intratumoural and peritumoural areas. Data are presented as median with *IQR*. A Mann–Whitney test was used to assess significance between the two groups ($n = 4$). *$p < 0.05$. **(e)** Schematic overview of the application of locoregional ^{211}At TAT targeting SDC1. C57BL/6JRj mice received an orthotopic graft of 50,000 GL261 cells in the right striatum by stereotaxis. After MRI confirmation of tumour uptake, the 9E7.4 mAb labelled with ^{211}At was injected on d11 at the same coordinates by CED. Mice were subsequently monitored weekly by MRI. Blood toxicity was assessed on a weekly basis. Renal and hepatic toxicity were monitored monthly. Illustration made with BioRender (biorender.com).

95% for *in vivo* experiments (Table S1) and its affinity was confirmed by flow cytometry (Fig. S1).

The 9E7.4 mAb enables a prolonged and localised cerebral retention of ^{125}I in tumour-bearing mice

We assessed the relevance of a locoregional therapeutic approach by evaluating the duration of cerebral retention of the radiolabelled 9E7.4 mAb. Due to limited availability and short half-life of ^{211}At, 9E7.4 and its isotype control (IgG2a, κ) were labelled with iodine-125 (^{125}I) to mimic the fate of ^{211}At in the biodistribution study, as these two radiohalogens share close physicochemical properties and similar biodistribution profiles.[39]

Tumour-bearing C57BL/6JRj mice underwent a striatal CED administration of ^{125}I-9E7.4 or ^{125}I-IgG2a, κ on d11. Mice were sacrificed and organs were harvested 2, 7, 21, and 72 h post-injection (n = 3 for each). The radioactivity in each organ was measured in a gamma counter. CED administration of both radiolabelled 9E7.4 and IgG2a, κ demonstrated predominant cerebral retention (Fig. 2a and b). A comparative biodistribution of the two radioconjugates revealed a higher cerebral retention of ^{125}I-9E7.4 than IgG2a, κ throughout the 2–72 h period (Fig. 2c). This retention profile was, thus, consistent with the 7.2-h half-life of ^{211}At. A moderate retention of ^{125}I-9E7.4 was also observed in the spleen, small intestine, and liver. The biodistribution study for each

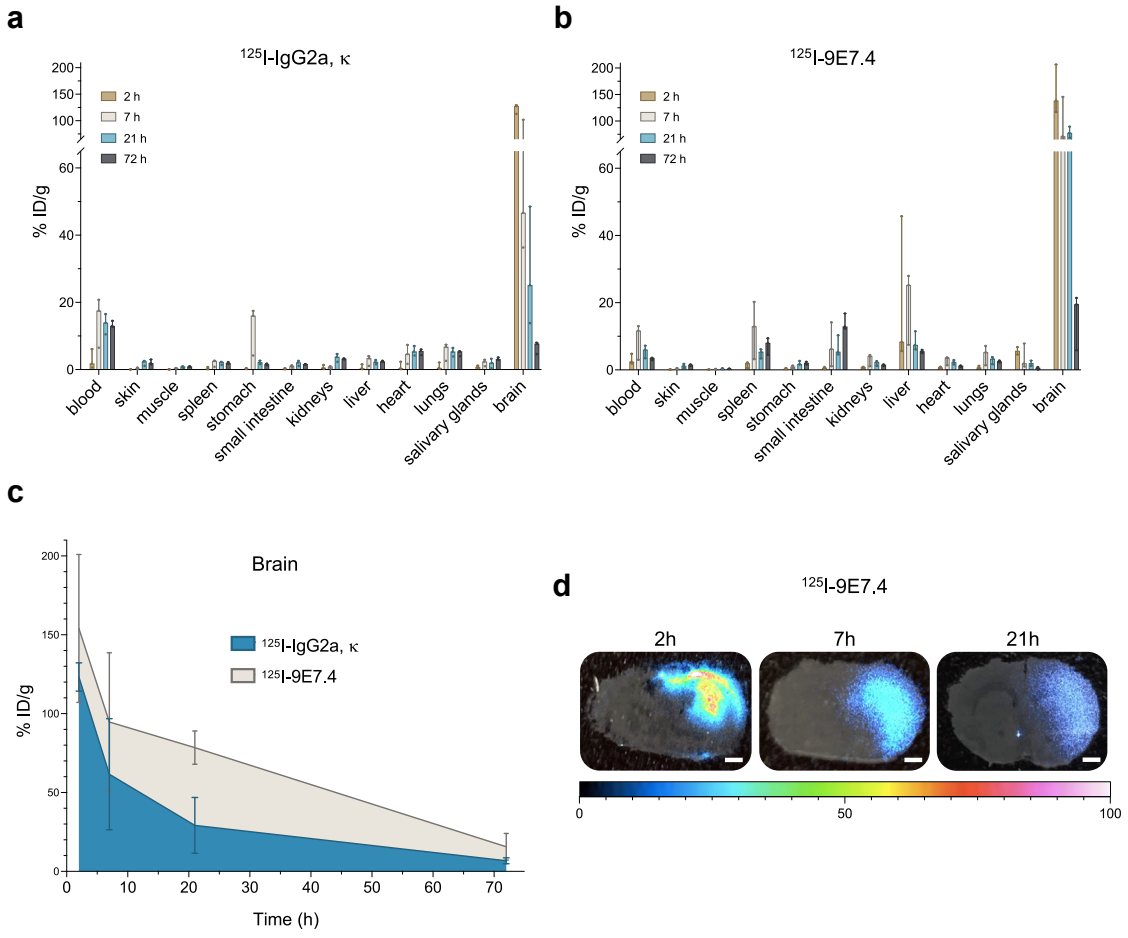

***Fig. 2:* The 9E7.4 mAb enables a prolonged and localised cerebral retention of ^{125}I in tumour-bearing mice.** **(a and b)** Biodistribution analysis conducted on (**a**) ^{125}I-IgG2a, κ and (**b**) ^{125}I-9E7.4 conjugates. 2.8 μg of mAb were labelled with 30 kBq of ^{125}I. C57BL/6JRj mice were stereotactically injected with 50,000 GL261 cells into the right striatum on d0. On d11, mice were administered a CED injection of the radioconjugates at the same coordinates and sacrificed after 2 h, 7 h, 21 h or 72 h. n = 3 for each time point. Data are expressed as a percentage of injected dose per gram (%ID/g) and presented as median with *IQR*. **(c)** Comparative biodistribution of ^{125}I-IgG2a, κ and ^{125}I-9E7.4 in the brain between 2 h and 72 h after locoregional CED injection in GB-bearing C57BL/6JRj mice (n = 3 for each time point). Radioconjugates were injected 11 days after tumour graft. Data are shown as a percentage of injected dose per gram (%ID/g) and presented as mean ± *SD*. **(d)** Digital autoradiography performed on mouse brains at 2 h, 7 h or 21 h after ^{125}I-9E7.4 injection in GB-bearing C57BL/6JRj mice. n = 3 for each time point. Scale bar = 1 mm.

organ is available in the Supplementary Data (Fig. S2). A dosimetry study based on these data allowed for the estimation of the absorbed dose of ^{211}At. Thus, for an injected activity of 100 kBq of ^{211}At-9E7.4, the absorbed dose in the brain is 4.35 Gy compared to 2.78 Gy for ^{211}At-IgG2a, κ (Table S3).

We visualised the brain distribution of ^{125}I-9E7.4 by digital autoradiography of brain cryosections produced under the same experimental conditions (n = 3 for each time point). These images displayed a high concentration of radioactivity 2 h post-injection, confined to the area of tumour cell injection. Within 7 h following the administration of ^{125}I-9E7.4, the area of distribution had expanded within the ipsilateral cerebral hemisphere without complete coverage and never reached the contralateral hemisphere. After 21 h, equivalent to three ^{211}At half-lives, measurable activity persisted within the same extended area (Fig. 2d).

Locoregional treatment of GB with ^{211}At-9E7.4 TAT leads to improved survival and minimal toxicity

We investigated the preclinical effects of ^{211}At locoregional therapy for GB by exploring the hypothesis of the targeting of SDC1. The lethal dose of ^{211}At for 10% of animals (LD_{10}) was previously established at 46 MBq/g for an intravenous injection of ^{211}At-labelled mAb in female mice,[40] equivalent to 920 kBq for a 20 g mouse. As we were conducting a study of intracranial administration of ^{211}At in mice, we hypothesised that the TAT could be effective with a significantly lower activity than intravenous preclinical tests,[22–24] leading us to set the highest injected activity at 470 kBq in our study. After confirming GB presence by MRI on d11, three groups of mice received a single CED injection of ^{211}At-9E7.4: 470 kBq (n = 5), 200 kBq (n = 16), or 100 kBq (n = 10). As a control, injection of 100 kBq of ^{211}At-IgG2a, κ (n = 5), 100 kBq of unlabelled ^{211}At ([^{211}At]NaAt; n = 4), and 2.8 μg of unlabelled 9E7.4 mAb (n = 6) were tested. Untreated mice received an injection of saline solution (0.9% NaCl; n = 15). Mice were euthanised upon weight loss exceeding 20% of initial weight, combined with the deterioration of general condition and the appearance of significant pain symptoms like reduced activity, reduced food and drink intake, orbital tightening, abnormal ear position, aggression and vocalisation (Fig. 1e).

All three tested activities showed striking efficacy in contrast to a median overall survival of 34 days for untreated animals. P-values were determined with a Log–Rank test, and HR and 95% CI with a Cox proportional hazards regression. After 162 days, the survival rate of mice that received 470 kBq was 60% (3/5; $^{*}p$ = 0.0225, HR = 0.12, 95% CI: 0.02–0.48), the survival rate of those that received a 200 kBq injection was 44% (7/16; $^{***}p$ = 0.0003, HR = 0.17, 95% CI: 0.06–0.42), and the survival rate of those that received a 100 kBq injection was 70% (7/10; $^{****}p$ < 0.0001, HR = 0.09, 95% CI: 0.02–0.29). None of the control conditions had a significant impact on the survival of the animals relative to the untreated group (Fig. 3a, Table S4). Weight had no impact on the outcome of the study (p = 0.3647, Cox proportional hazards regression).

Weight loss was monitored on a weekly basis to evaluate treatment-induced toxicity. With the exception of a minor transient decline post-treatment, the therapy did not affect the weight (Fig. 3b–d). Individual data of weight monitoring is available in the Supplementary Data (Fig. S3). In long-term survivors treated with 200kBq and 100 kBq, we observed no significant haematological impairment as evidenced by stable erythrocytes (Fig. 3e), leukocytes (Fig. 3f), and platelets (Fig. 3g) levels up to the end of the study. The 470 kBq activity exhibited a transient decrease in erythrocytes and platelets at d42–47, below toxicity threshold provided by our haematology analyser (Fig. 3e–g). Blood levels of lymphocytes, monocytes, neutrophils, eosinophils, basophils and hemoglobin were also monitored and did not exhibit any significant variation associated with toxicity (Fig. S4), except for a transient hemoglobin decrease at d42–47 in mice treated with 470 kBq (Fig. S4f). Decreasing trends in erythrocyte counts and hemoglobin levels were observed on d11 in groups treated with ^{211}At alone and with IgG2a, κ (Fig. S5). Individual haematology follow-up for TAT-injected mice sacrificed during the survival study is available in the Supplementary Data (Fig. S6).

Regarding the hepatic enzymes alanine aminotransferase (ALT) and alkaline phosphatase (ALP), no significant increase associated with toxicity was detected for the three activities (Fig. 3h and i). Creatinine level, indicating kidney status, did not show any variation (Fig. 3j). We also assessed blood levels of glucose, phosphate, total proteins, albumin, globulin, bilirubin, and calcium. The values remained below the thresholds associated with systemic toxicity (Fig. S7). Individual data for the control groups and for TAT-injected mice sacrificed during the survival study are available in the Supplementary Data (Fig. S8, Fig. S9).

Activity-dependent radionecrosis resolves over time only in the case of a 100 kBq injection of TAT

We monitored tumour growth and studied the direct effects of α radiations on the brain tissue by MRI. The T2-weighted axial MRI images showed established tumours in control groups after d11 (Fig. 4a), whereas mice treated with ^{211}At-9E7.4 TAT exhibited an activity-related hypersignal similar to that of radionecrosis (Fig. 4b). The simultaneous acquisition of T1-weighted MRI images confirmed the presence of free water in the injection area (Fig. S10a and b). These areas decreased over time until stabilising. Interestingly, it only occurred when associating ^{211}At with the 9E7.4 mAb. Despite its efficacy, the 470 kBq activity was subsequently discontinued in the ensuing series due to the severity of the radionecrosis induced by the treatment.

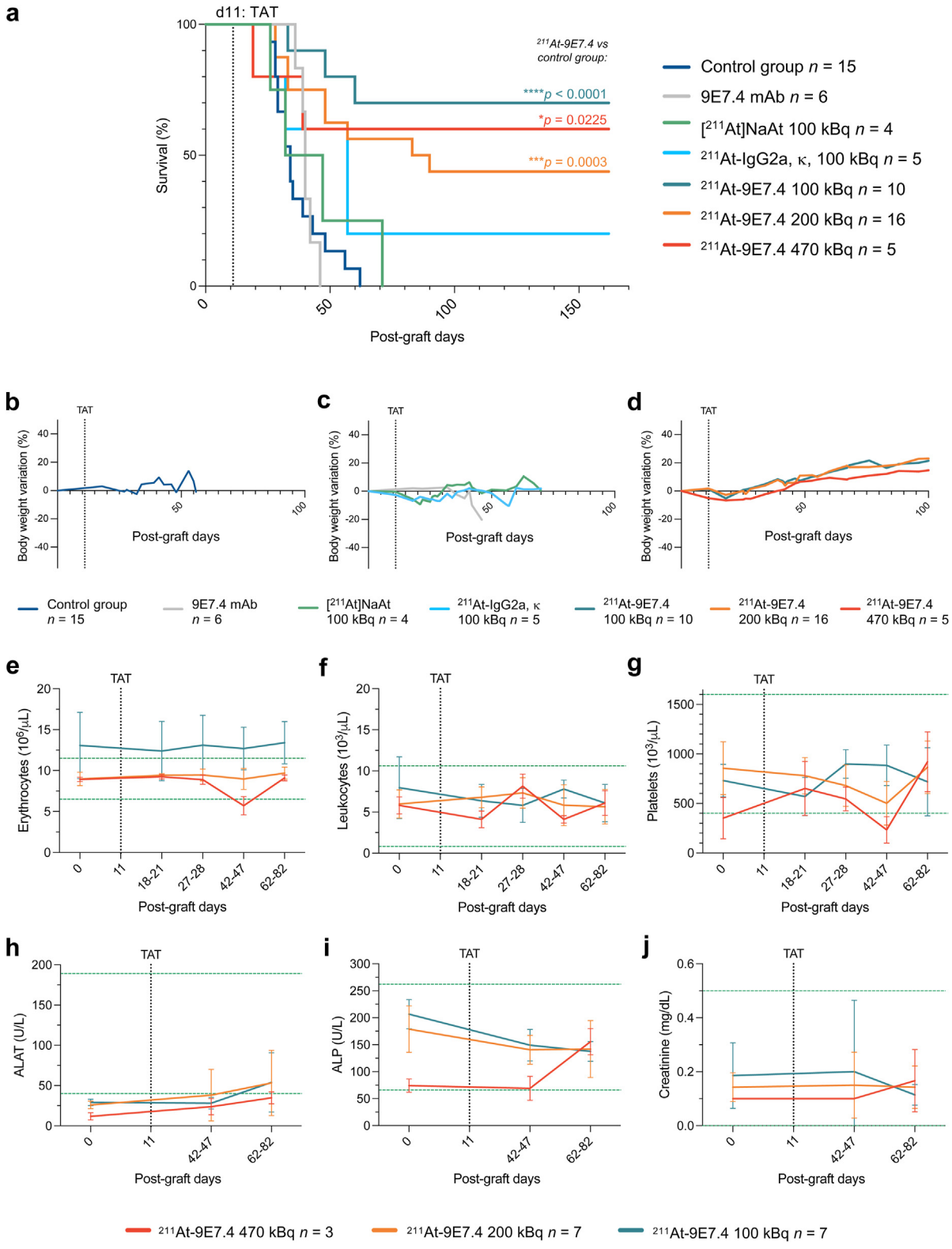

Fig. 3: **Locoregional treatment of GB with ^{211}At-9E7.4 TAT leads to improved survival and minimal toxicity. (a)** Kaplan–Meier survival curves. C57BL/6JRj mice were injected at d0 with 50,000 GL261 cells into the right striatum. After validation of tumour presence by MRI, mice received at d11, at the same coordinates, a CED injection

Reduced tumour growth in the ^{211}At-IgG2a, κ condition was also observed, even though four out of five mice eventually succumbed to their tumour (Fig. 4c, Fig. S10f). The determination of tumour volumes also confirmed a strong growth inhibition in TAT conditions (Fig. 4d, Fig. S10g–i). The calculation of radionecrosis volumes in long-term survivors confirmed their reduction towards stable dimensions and their proportionality to the injected activities. At the end of the follow-up, mice treated with 470 kBq had an average volume of radionecrosis of 16 ± 5.5 mm^3, and those treated with 200 kBq had an average volume of necrosis of 4 ± 3.8 mm^3, whereas it was no longer detectable in survivors treated with 100 kBq (Fig. 4e). A summary of the survival study can be found in the Supplementary Data (Tables S5 and S6).

Locoregional ^{211}At-9E7.4 TAT decreases the occurrence of secondary tumours

In an independent cohort of mice, we studied the direct effects of TAT on locoregional tumour expansion by histology. We followed the same protocol as for the survival study with a single CED injection at d11 of ^{211}At-9E7.4 (200 kBq, n = 4; 100 kBq, n = 4) or saline solution (0.9% NaCl, n = 4). Mice were sacrificed at d18, seven days after injection of the TAT.

Histopathological analyses carried out on brain cryosections revealed the presence of tumour cell foci in both ventricles at d18 in 100% of control mice and 87.5% of treated mice, although each group showed strong heterogeneity (Table S7). In control mice, we detected substantial proliferation of tumour cells in the striatum, with the presence of large and atypical glial cells. In addition, tumour cells were identified within the right (RV) and left (LV) ventricular regions (tumour cells in RV: 3/4, in LV: 4/4). In mice treated with 200 kBq, necrotic material at the site of injection was observed, corroborating the radionecrosis previously detected by MRI (Fig. 4b). Tumour cells were also discerned in both ventricular zones (tumour cells in RV: 4/4, in LV: 1/4). Mice injected with 100 kBq showed moderate chronic lymphocytic infiltrates and very few radionecrosis. They also exhibited tumour foci in both ventricles, excepted in one case (tumour cells in RV: 2/4, in LV: 3/4; Fig. 5a, Table S7).

In the survival study, the MRI resolution was insufficient to distinguish such foci at d18. However, we identified the development of a secondary tumour located next to the hypothalamus from d25 in some mice within each group (Fig. 5b). 60% of the untreated mice succumbed to this type of tumour mass whereas this incidence was reduced in mice treated with TAT: 20% (1/5) for the 470 kBq activity, 44% (7/16) for the 200 kBq activity, and 20% (2/10) for the 100 kBq activity (Fig. 5c).

Locoregional ^{211}At-9E7.4 TAT elicits vascular remodeling and local inflammation after seven days

We studied the responses of the tumour environment by immunofluorescence analysis on brain sections. The same protocol as for the survival study was used. At d11, mice received a single CED injection of 200 kBq of TAT (n = 4) or saline solution (0.9% NaCl; n = 4), and were sacrificed at d18. We studied two areas of the brain: the injection area in the striatum (S) and the area adjacent to the right ventricle (V). Here, our aim was to assess responses of three components of the GB microenvironment: vasculature, inflammation, and adaptative immunity. Given the known effects of radiation on blood vessels, we performed CD31 labelling. Markers of innate immunity were also investigated: CD45 for all leukocytes, and CD11b for monocytes/macrophages, granulocytes, and NK cells. T cells were detected by CD3, CD4, and CD8 staining.

Immunofluorescence staining revealed a size increase of CD31$^+$ blood vessels in mice treated with TAT (Fig. 6a). Quantification of the fluorescence indicated a superior CD31$^+$ expression in these vessels compared to brain sections of control mice. This observation was significant in the injection area (*p = 0.028571) and followed the same trend in the area adjacent to the right ventricle (*p = 0.028571; Fig. 6b). In addition, the number of vessels was significantly lower in these two areas for mice treated with TAT (*p = 0.028571; Fig. 6c).

High expression of CD45 and CD11b indicated an increase in the local inflammatory infiltrate (Fig. 6d). In treated mice, CD11b quantification showed a significantly higher expression at the injection site (*p = 0.028571) but not in the area adjacent to the right ventricle. Very few T cells were detected in the brain tissue and no significant difference was observed regarding the fluorescence levels of CD3, CD4 and CD8 measured in both areas (Fig. 6e).

Locoregional ^{211}At-9E7.4 TAT protects the brain from contralateral tumour injection

Given the extensive research on immune responses induced by ionising radiation, we investigated if

of ^{211}At-9E7.4 (470, 200 or 100 kBq), ^{211}At-IgG2a, κ (100 kBq), [^{211}At]NaAt (100 kBq), unlabelled 9E7.4 mAb (2.8 μg) or saline solution (0.9% NaCl) in a volume of 5 μL. A Log–Rank test was used to establish statistical significance in comparison with the control group. *p < 0.05, ***p < 0.001, ****p < 0.0001. **(b–d)** Weight curves of **(b)** the control group, **(c)** non-targeting groups (^{211}At-IgG2a, κ, [^{211}At]NaAt, unlabelled 9E7.4 mAb), and **(d)** groups treated with ^{211}At-9E7.4. Data are presented as mean. **(e–j)** Monitoring of blood toxicity. **(e)** Erythrocytes, **(f)** leukocytes, and **(g)** platelets levels were analysed with a quantitative haematology analyser. **(h)** Alanine aminotransferase (ALAT), **(i)** alkaline phosphatase (ALP), and **(j)** creatinine levels were measured with a chemistry analyser. Data are presented as mean ± *SD*. Dotted green lines indicate toxicity thresholds provided by the devices for C57BL/6JRj mice.

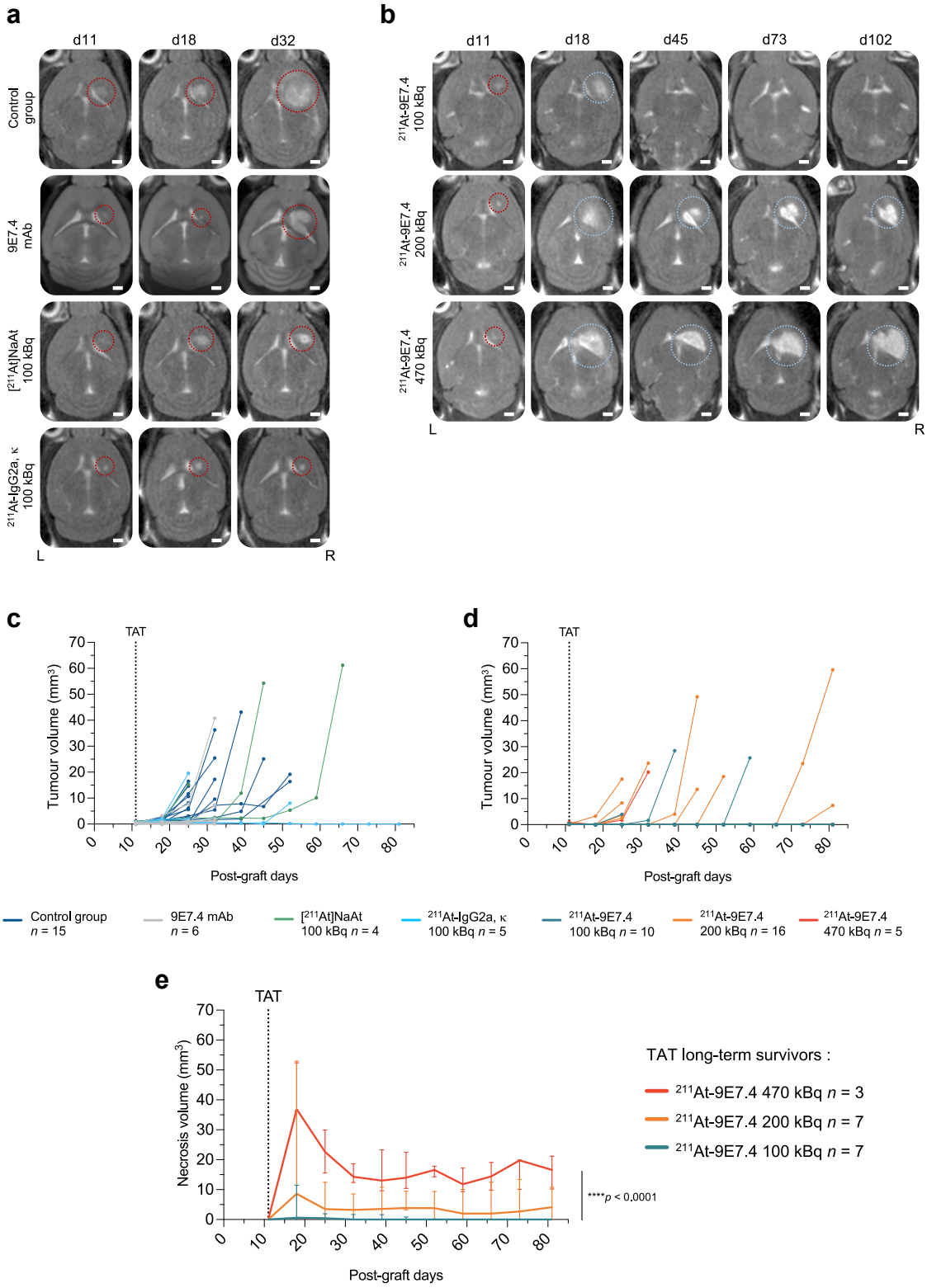

Fig. 4: **Activity-dependent radionecrosis resolves over time only in the case of a 100 kBq injection of TAT. (a and b)** Axial T2-weighted MRI brain images of C57BL6/JRj mice from the survival study. Tumour-bearing mice were injected at d11 with **(a)** saline solution (0.9% NaCl;

antitumour immunity was operational in long-term survivors. Immune responses could indeed contribute to reduce the development of secondary tumours by eliminating cells migrating from the primary implantation site. 15 of the 17 long-surviving mice were rechallenged on d162 with a contralateral graft of 50,000 GL261 cells, divided into the following groups according to their previous treatment: 470 kBq, $n = 3$; 200 kBq, $n = 6$, and 100 kBq, $n = 6$. The new graft was placed in the striatum of the contralateral hemisphere, which had not been previously exposed to ^{211}At radiations (Fig. 2b). Follow-up was performed by weekly MRI.

Remarkably, 93% (14/15) of the rechallenged mice survived for 100 more days: $^{**}p = 0.0042$ in the 470 kBq group, $^{***}p = 0.0001$ in the 200 kBq group, and $^{***}p = 0.0001$ in the 100 kBq group (Log–Rank test; Fig. 7a). Weight had no impact on the outcome of the study ($p = 0.1750$, Cox proportional hazards regression). Weight tracking indicated that the long-term survivors tolerated the surgical intervention and were still able to gain weight (Fig. 7b, Fig. S11a–d). In all rechallenged mice, no tumour was detected by MRI (Fig. 7c and d). The TAT-induced radionecrosis (Fig. 4b) was still visible in mice previously treated with 470 and 200 kBq and remained undetectable in the 100 kBq group (Fig. 7d, Fig. S11e). To detect tumour growth, the cerebral uptake of [^{18}F]FDG was assessed by positron emission tomography (PET) in an untreated mouse and two long-term survivors previously treated with 200 and 100 kBq of TAT, respectively. In the control mouse, a strong [^{18}F]FDG accumulation confirmed the presence of a tumour that was detected in T2-weighted images (Fig. 7e). In the rechallenged mice, no [^{18}F]FDG fixation was detected at d34 in the injection site nor in the radionecrosis area (Fig. 7f). A summary of this study is available in the Supplementary Data (Tables S8 and S9).

Locoregional ^{211}At-9E7.4 TAT elicits the activation of immune memory

With the aim of detecting memory T cells associated with this long-term protection, whole blood cytometry was assessed in a fraction of rechallenged mice ($n = 5$) and control mice ($n = 6$) at three time points (d4, d7, and d10 after the contralateral tumour graft). The rechallenged subset included mice treated with 200 kBq ($n = 3$) and 100 kBq ($n = 2$) of TAT, given that they met the criterion of surviving beyond 162 days post-initial transplantation. From the CD45$^+$/CD3$^+$ blood population, we investigated the CD4$^+$ and CD8$^+$ central memory T phenotypes (CD44$^+$/CD62L$^+$; T_{CM}) and effector phenotypes (CD44$^+$/CD62L$^-$; T_{EM}).

At d4, a larger number of CD3$^+$ T_{CM} was detected in rechallenged mice compared to the control group ($^*p = 0.012931$). This phenomenon only relied on CD8$^+$ T_{CM} ($^*p = 0.012931$) and not on CD4$^+$ T_{CM}. By d10, in rechallenged mice, CD4$^+$ T_{CM} increased in number while CD8$^+$ T_{CM} declined by d7. In control mice, CD4$^+$ T_{CM} level remained stable over time and CD8$^+$ T_{CM} increased by d7 (Fig. 8a). We also detected a larger number of CD3$^+$ T_{EM} at d4 in the rechallenged mice than in the controls ($^*p = 0.02575$). In this case, both CD4$^+$ and CD8$^+$ T_{EM} phenotypes were responsible for this observation; by d7, both phenotypes started to decline. In control mice, only a slight increase of CD4$^+$ T_{EM} was detected by d10 (Fig. 8b). Additional information about the monitoring of CD44$^-$/CD62L$^+$ naïve and CD44$^-$/CD62L$^-$ T cells is available in the Supplementary Data (Fig. S12).

Discussion

In the GB clinical landscape, TAT is typically explored after surgical resection and application of the Stupp regimen,[16,18,19] although chemotherapy and external radiotherapy promote radioresistance in residual GB cells.[4,5] To bypass these constraints, we aimed to evaluate the efficacy of locoregional ^{211}At-9E7.4 TAT on an unresected and untreated orthotopic GB mouse model. In addition, the presence of the tumour could enhance the retention of TAT and help to reach infiltrative cells. The feasibility and safety of this kind of approach was previously demonstrated by Cordier et al. in a pilot study involving five patients with GB.[17]

In this study, a single injection of ^{211}At-9E7.4 TAT was able to generate long-term survivors, with the 100 kBq activity achieving the best survival rate of 70%. In contrast, the recapitulation of a Stupp-like regimen in the orthotopic C57BL/6JRj-GL261 model reaches a survival median of 60 days,[41] underlying the strong benefit of TAT as a first-line approach.

We observed activity-dependent radionecrosis in our TAT protocol (Fig. 4b and e), indicating significant cerebral toxicity at 470 kBq, persistent yet unresolved radionecrosis at 200 kBq, and resolution in the 100 kBq group, likely due to compensation by surrounding

$n = 15$), ^{211}At-IgG2a, κ ($n = 4$), [^{211}At]NaAt ($n = 5$), unlabelled 9E7.4 mAb ($n = 6$), **(b)** 470 kBq ($n = 5$), 200 kBq ($n = 16$), or 100 kBq ($n = 10$) of ^{211}At-9E7.4. Brightness and contrast have been adjusted for clarity. Red circles indicate tumour presence. Blue circles indicate radionecrosis. L: left. R: right. Scale bar = 1 mm. **(c** and **d)** Individual tumour volumes measured from MRI images in **(c)** non-targeting groups (^{211}At-IgG2a, κ, [^{211}At]NaAt, unlabelled 9E7.4 mAb), and **(d)** groups treated with ^{211}At-9E7.4. Data are presented as mean ± *SD*. **(e)** Volumes of radionecrosis measured from MRI images in long-term survivors treated with 470 kBq ($n = 3$), 200 kBq ($n = 7$) or 100 kBq ($n = 7$) of ^{211}At-9E7.4. Data are presented as median with IQR. A Friedman test with post hoc Dunn correction for pairwise comparisons was performed to assess significance between each group. $^{****}p < 0.0001$.

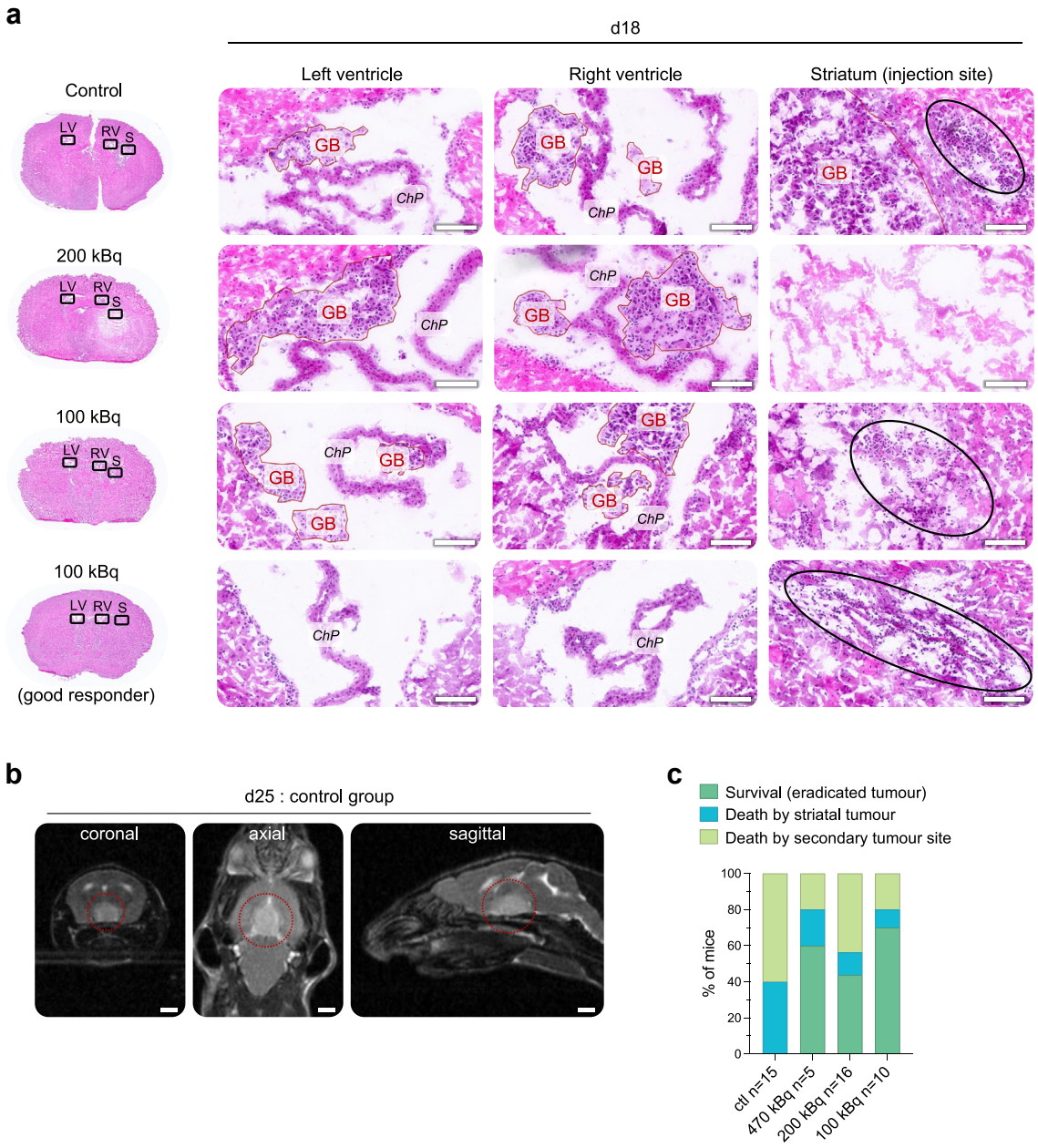

Fig. 5: **Locoregional ^{211}At-9E7.4 TAT decreases the occurrence of secondary tumours. (a)** Histological analysis of tumour-bearing mouse brains treated with 200 kBq or 100 kBq of ^{211}At-9E7.4, or injected with saline solution (0.9% NaCl; *n* = 4 for each group). C57BL/6JRj mice were injected at d0 with 50,000 GL261 cells into the right striatum. At d11, they received at the same coordinates a CED injection of TAT or saline solution (0.9% NaCl). Mice were euthanised 18 days post-tumour grafting (seven days post-TAT). Tumour cells are delineated with a red line. Black circles indicate inflammation zones. LV: left ventricle. RV: right ventricle. S: striatum. GB: glioblastoma. ChP: choroid plexus. Scale bar = 100 µm. **(b)** T2-weighted MRI of a control mouse brain from the survival study displaying a secondary tumour indicated by a white arrow. Scale bar = 2 mm. (**c**) Overview of the survival/death ratio and types of induced tumours (striatal or secondary tumours) during the survival study in relation to the injected activity of ^{211}At-9E7.4 (470, 200 or 100 kBq).

healthy tissues. Radionecrosis after a ^{211}At TAT injection was already described in Zalutsky et al.'s clinical trial, but no patient required surgery.[16] Transient radionecrosis could thus assist in tumor demarcation for resection surgery.[17] Additionally, activities of 200 kBq and 100 kBq showed no blood toxicity, while

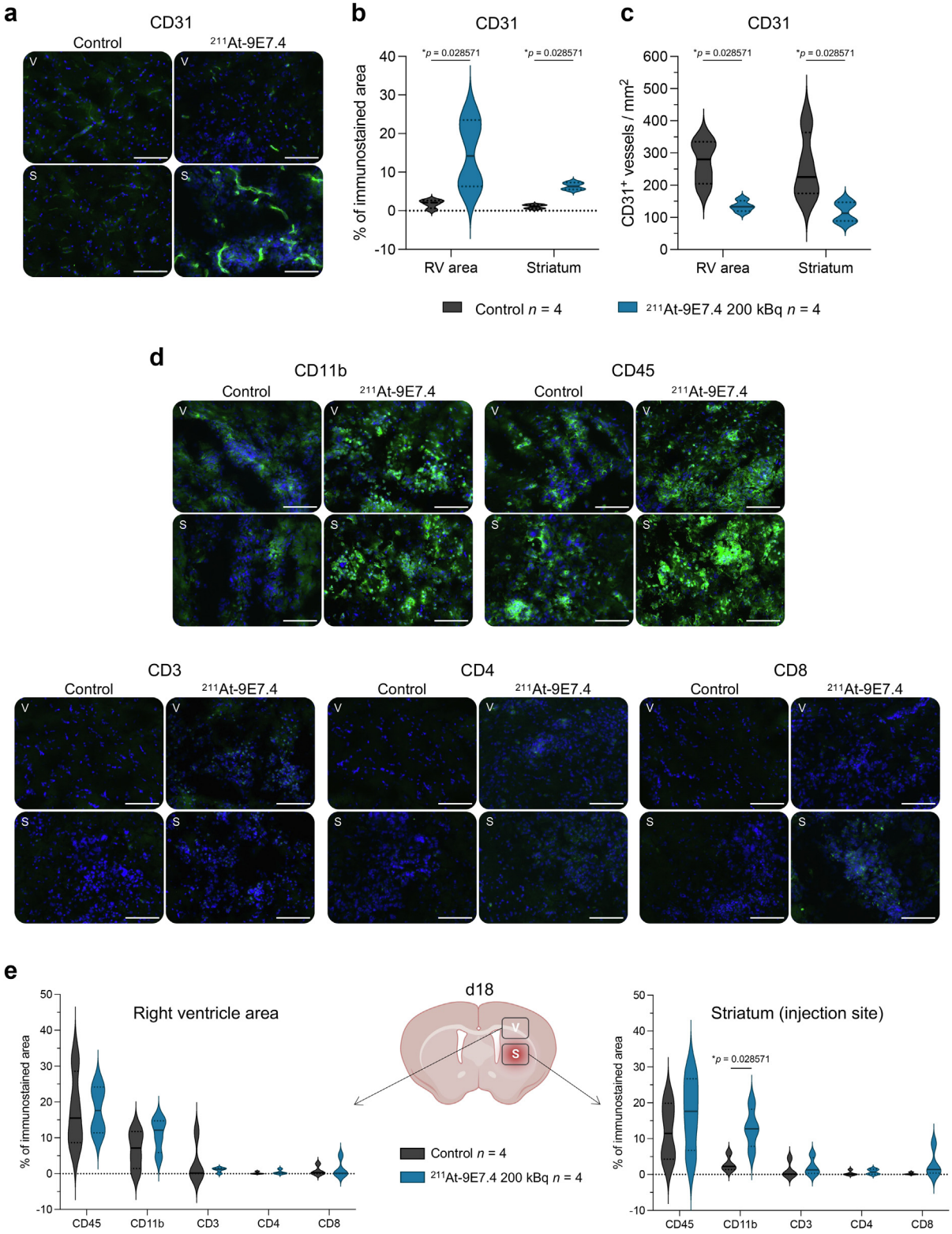

Fig. 6: **Locoregional ^{211}At-9E7.4 TAT elicits vascular remodeling and local inflammation after seven days. (a)** Immunofluorescence labelling of CD31 in mouse brain cryosections. GB-bearing mice were injected with 200 kBq of ^{211}At-9E7.4 (n = 4) or saline solution (0.9% NaCl, n = 4) at d11. Mice were sacrificed at d18 (seven days post-

transient fluctuations above toxicity thresholds were detected at 470 kBq (Fig. 3e and g). Exploring fractionation or a single injection of an activity lower than 100 kBq could be beneficial in this model. Nevertheless, further investigation into cerebral toxicity through behavioral and cognitive experiments is warranted to assess brain function even after radionecrosis resolution. Given the locoregional injection and targeting of SDC1, this approach suggests a significant reduction in injected dose compared to intravenous TAT approaches to achieve therapeutic efficacy. Thus, the 100 kBq activity displays both the highest survival rate and the lowest toxicity. This also represents the lowest activity ever tested for ^{211}At *in vivo* in a GB model. Conversely, prior preclinical investigations used activities ranging from 180 kBq to 1.11 MBq of ^{211}At in subcutaneous GB mouse models, yet without a curative outcome.[23–25,27,28]

The SDC1-dependent brain retention of TAT proved to be essential for tumour eradication, as only mice treated with ^{211}At-9E7.4 became long-survivors (Fig. 3a). It resulted in a reduced distribution in peripheral organs compared to the intravenous injections that we previously assessed with ^{211}At-9E7.4.[29] Although liver, spleen, and small intestine exhibit substantial expression of SDC1,[42–44] no related toxicity was detected (Fig. 3e–i, Figs. S4 and S7). In this context, the ^{211}At-9E7.4 TAT is revealed as a highly sensitive system, requiring a minimal amount of 9E7.4 mAb (down to 0.56 µg per mouse, equivalent to 28 µg/kg) to retain ^{211}At within the tumour. By comparison, efficient mAb concentrations in systemic and intracranial approaches for GB vary from 5 to 10 mg/kg.[45,46] Contrary to current systemic modalities that require low molecular weight vectors with short biological half-lives to overcome the BBB and minimise systemic toxicity, the elevated molecular weight (~150 kDa) and extended half-life of mAbs stand as favorable properties to achieve therapeutic efficacy in a locoregional context.

Despite the eradication of orthotopic tumours in long-term survivors, ventricular tumour foci were detected on d18 in distinct cohorts of treated mice (Fig. 5 and Table S7). This raises questions regarding their fate in the long-survivors, as they remained undetected by MRI during the monitoring period. Conversely, hypothalamic tumours developed from d25 in some mice of each group of the survival study (Fig. 5b). This observation is consistent with the ability of the GL261 cell line to generate secondary tumours after an intra-striatal injection,[47] thereby mirroring multifocal GBs observed in 17.2% of patients.[48] The presence of hypothalamic tumours in our model supports the hypothesis of GB cell migration through the cerebrospinal fluid after contact with the ventricles and the subventricular zone (SVZ) during the growth of the primary tumour. Therefore, the ventricular tumour foci observed at d18 could be the origin of these hypothalamic tumours. In the survival study, hypothalamic tumours accounted for the mortality of 60% of the control group. In treated mice, this death rate dropped to 20% in the 470 kBq and 100 kBq groups, and to 44% in the 200 kBq group, highlighting an inhibitory effect of TAT on secondary tumour occurrence (Fig. 5c). In patients, irradiation of neural stem cells (NSCs) of the SVZ inhibits the migration of GB stem-like cells (GSLCs).[49] In our protocol, the SVZ in the right hemisphere was subjected to TAT irradiation (Fig. 2b), which could directly impact the influence of NSCs on GB migration towards the hypothalamus.

In addition, SDC1 is primarily expressed in the choroid plexus of the brain[50] and plays a crucial role in stimulating adult neurogenesis by increasing the proliferation of NSCs in the SVZ.[51] Thus, its targeting could also contribute to reduce the activity of GSLCs. In GB, SDC1 performs distinct functions depending on its location (membrane-bound, nucleus-translocated, or soluble).[30] Given its regulation by NF-κB,[52] its overexpression in the GB mesenchymal phenotype,[53] and its ability to activate pro-EMT genes such as NF-κB and TGF-β in different cancers,[54] it may have a role in modulating the epithelial-to-mesenchymal transition (EMT) in GB. Its soluble form is also involved in the formation of protein complexes capable of activating radioresistance pathways.[33] These functions may be altered through the application of the 9E7.4 mAb, restricting its shedding, internalisation, and membrane interactions, thereby contributing to a reduced migratory and radioresistant capacity of the tumour. These hypotheses are strengthened by the fact that we observed no secondary tumours in the six mice treated with the 9E7.4 mAb alone, in addition to their reduced occurrence in response to ^{211}At-9E7.4 TAT (Table S5).

These effects might also enable the full exploitation of the immunogenic power of TAT. Indeed, several *in vivo* studies reported the ability of α particles to trigger an immune response, such as the release of damage-associated molecular patterns (DAMPs) in an adenocarcinoma model,[55] increased production of interleukin-2 (IL-2), chemokine CC ligand 5 (CCL-5),

TAT). S: striatum area. V: right ventricle area. Scale bar = 100 µm. **(b)** Fluorescence quantification of the CD31 staining. Data are expressed in percentage of immunostained area and presented as median with IQR. A Mann–Whitney test was performed to assess significance between groups. *$p < 0.05$. **(c)** CD31$^+$ blood vessels counting. Data are expressed in number of CD31$^+$ vessels per mm^2 of tissue and presented as median with IQR. A Mann–Whitney test was performed to assess significance between groups. *$p < 0.05$. **(d)** Immunofluorescence labelling of CD45, CD11b, CD3, CD4 and CD8 in mouse brain cryosections. S: striatum area. V: right ventricle area. Scale bar = 100 µm. (**e**) Fluorescence quantification. Data are expressed in percentage of immunostained area and presented as median with IQR. A Mann–Whitney test was performed to assess significance between groups. *$p < 0.05$. Illustration made with BioRender (biorender.com).

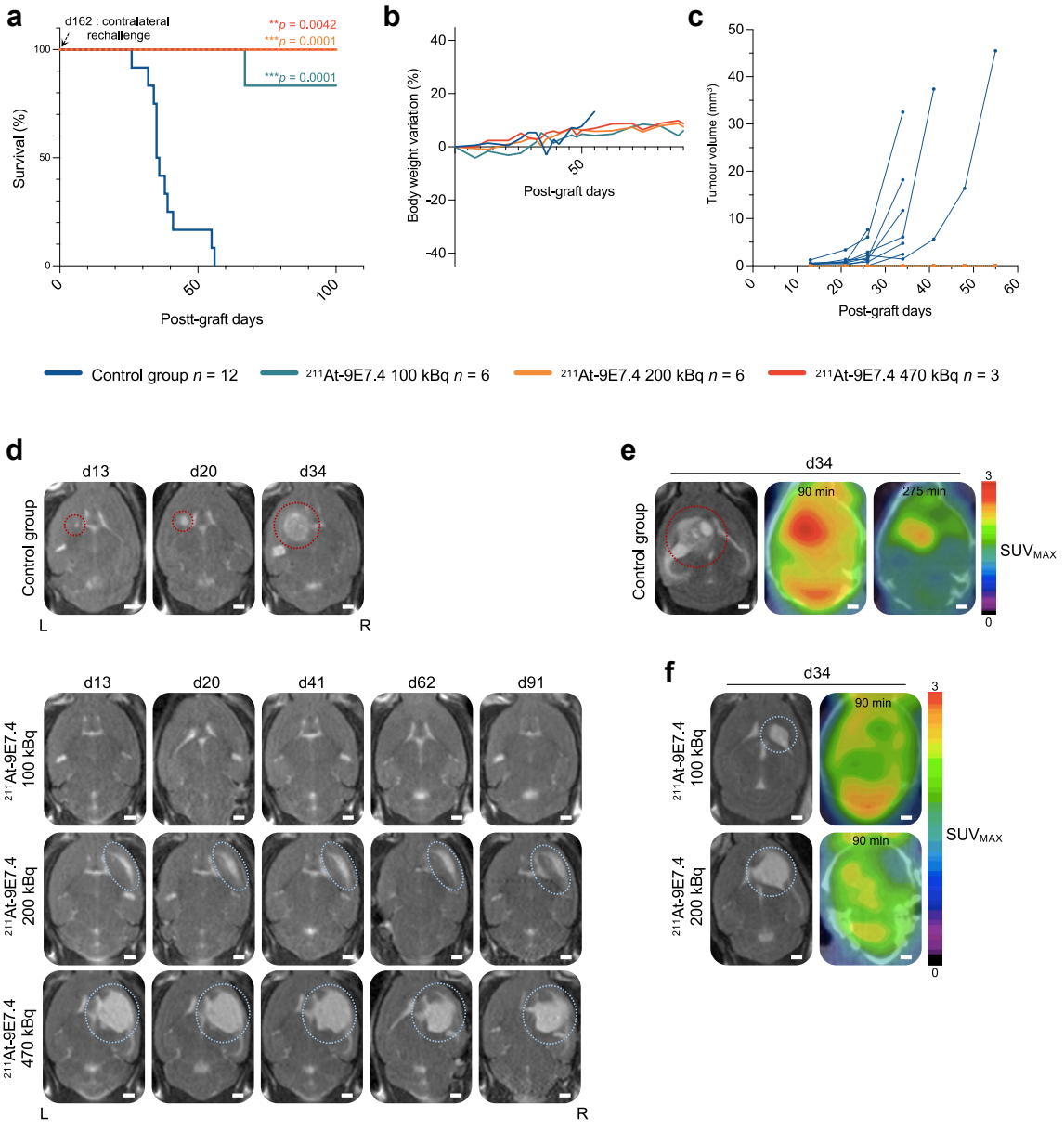

***Fig. 7*: Locoregional ^{211}At-9E7.4 TAT protects the brain from contralateral tumour injection. (a)** Kaplan–Meier survival curves. After 162 days of survival, 15 long-term survivors and 12 control mice were injected with 50,000 GL261 cells into the left striatum by stereotaxis. TAT injection at d11: 470 kBq (n = 3), 200 kBq (n = 6), 100 kBq (n = 6). Data come from three independent experiments. A Log–Rank test was used to establish statistical significance in comparison with the control group. $^{**}p < 0.01$, $^{***}p < 0.001$. **(b)** Percentage of initial weight variation. Data are expressed as mean. **(c)** Individual tumour volumes measured from MRI. **(d)** Axial T2-weighted MRI of brain in rechallenged mice. Brightness and contrast have been adjusted for clarity. Red circles indicate tumour presence. Blue circles indicate radionecrosis. L: left. R: right. Scale bar = 1 mm. **(e** and **f)** T2-weighted MRI and [^{18}F]fluorodeoxyglucose ([^{18}F]FDG) PET/CT scans of brain from **(e)** a control mouse and **(f)** two rechallenged mice (200 or 100 kBq of ^{211}At-9E7.4 as initial treatment) 34 days after the contralateral rechallenge. Images were acquired 90 min and 275 min after [^{18}F]FDG injection. Blue circles indicate radionecrosis. Scale bar = 1 mm. SUV_{MAX} = Maximal Standardised Uptake Value.

and interferon γ (IFNγ) in a multiple myeloma model,[56] or migration of dendritic cells and tumour infiltration of CD8$^+$ T cells in a colorectal carcinoma model.[57] In patients, a decrease of CD8$^+$ T cells expressing programmed death-ligand 1 (PD-L1) after irradiation[58] and an abscopal effect by the eradication of distant and

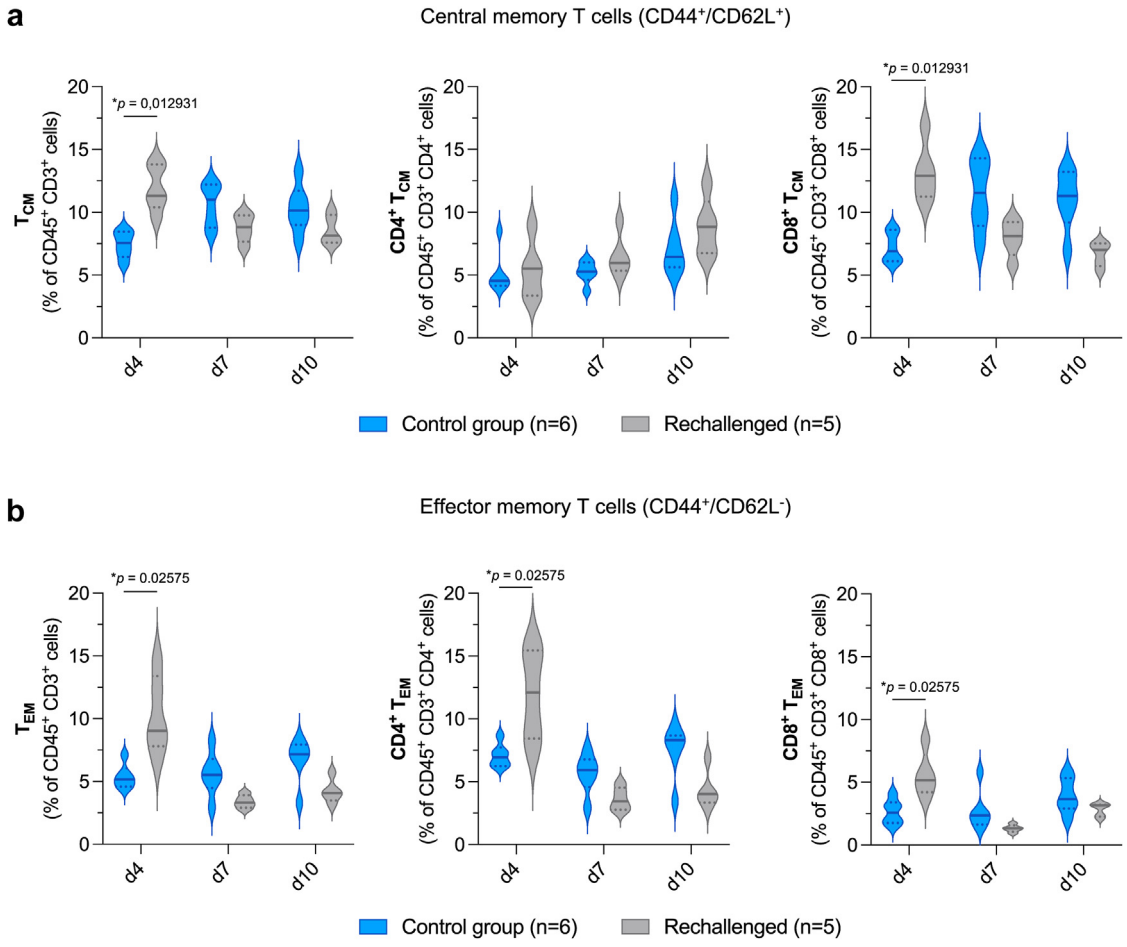

Fig. 8: **Locoregional ^{211}At-9E7.4 TAT elicits the activation of immune memory. (a)** Flow cytometry analysis of the central memory phenotype $CD44^+/CD62L^+$ among circulating $CD45^+/CD3^+$ T lymphocytes four, seven, and ten days after rechallenge. Central $CD4^+$ and $CD8^+$ phenotypes were also investigated. Data are expressed as median with *IQR*. Multiple Mann–Whitney tests were performed to assess significance between groups for each time point. $^*p < 0.05$. A Friedman test with *post hoc* Dunn correction for pairwise comparisons was performed to assess significance between each group. **(b)** Flow cytometry analysis of the effector memory phenotype $CD44^+/CD62L^-$ among circulating $CD45^+/CD3^+$ T lymphocytes four, seven, and ten days after rechallenge. Effector $CD4^+$ and $CD8^+$ phenotypes were also investigated. Data are expressed as median with *IQR*. Multiple Mann–Whitney tests were performed to assess significance between groups for each time point. $^*p < 0.05$. A Friedman test with *post hoc* Dunn correction for pairwise comparisons was performed to assess significance between each group.

untreated lesions have also been reported.[59] In our research, we noted vascular hypertrophy and significant $CD11b^+$ cell infiltration at d18 in treated mice. This hypertrophy suggests a disruption of the BBB, which could account for the heightened infiltration by peripheral $CD11b^+$ cells. These observations stand in contrast to the findings of Behling et al., who documented BBB remodeling accompanied by a reduction in CD31 expression in blood vessels after intravenous administration of TAT in a mouse model.[60] Our findings were limited by the analysis of the response at a single time point, and likely missed events occurring earlier. Consequently, we observed no significant response from the adaptive immune system at d18 (Fig. 6d and e).

However, the 93% long-term survival rate after contralateral rechallenge (Fig. 7) and the induction of memory immunity (Fig. 8) prove that adaptive immunity was indeed activated post-TAT. The establishment of this memory immunity is also a potential explanation for the reduction in spontaneously occurring secondary tumours observed in mice treated with TAT. Control mice exhibited a delayed increase in blood T_{CM}, also indicating a potential antigenic presentation following tumour graft, but no change in the number of T_{EM} was observed. In rechallenged mice, although both naïve T cells and T_{CM} are known to interact with antigens,[61] the significant increase in blood T_{CM} suggests that they predominantly facilitated antigen presentation.

Furthermore, T_{EM} are known to be redirected from the blood towards non-lymphoid organs following the cleavage of L-selectin (CD62L) on their surface. Thus, the decline in blood T_{EM} in rechallenged mice on d7 suggests a blood-to-tissue flow towards the newly grafted tumour cells. As the GL261 cell line is highly immunogenic,[62] future studies should use less immunogenic GB murine cell lines, such as SB28, to thoroughly evaluate the immunogenicity of ^{211}At and compare it between female and male mice. However, the GL261 remains a pertinent model due to its widespread use and invasive capacity. A longitudinal assessment of adaptive immune responses, including DAMPs release and cytokines secretion following treatment with ^{211}At-9E7.4 TAT, should also be conducted.

To take into account the GB microenvironment, especially the immunological aspects after the standard-of-care, the inclusion of ^{211}At-9E7.4 TAT in a protocol that combines tumour resection with the Stupp regimen would be instrumental to pinpoint the optimal therapeutic timeframe for TAT efficacy. In addition, exploring therapeutic combinations could further enhance outcomes in both inoperable tumour and resection cavity. Specifically, when used in conjunction with immune checkpoint inhibitors, early immune responses could be amplified and further reduce the formation of secondary tumour foci, as shown in breast and colon cancer models by association of ^{211}At with anti-PD-L1.[63] Combination to chimeric antigen receptor T cells (CAR-T cells) or dendritic cell vaccine could also contribute to eradicate distant foci of tumour cells.[64,65] Finally, association of TAT with DNA repair inhibitors has recently been suggested to be an efficient way to improve therapeutic efficacy.[66]

Currently, both preclinical and clinical therapeutic studies on GB are focused on improving surgical resection and using both systemic and local approaches with chemotherapy, radiotherapy, and immunotherapy,[67] but the outcomes have not been satisfactory yet. While TAT has demonstrated remarkable results in other tumour models,[68] the outcome for GB has remained non-curative.[22,24,28] ^{211}At-9E7.4 is therefore one of the most effective TAT in the GB preclinical landscape. This study has the advantage of presenting an orthotopic approach to highlight the benefits of locoregional therapy for GB, as subcutaneous models poorly replicate the GB microenvironment. Additionally, using a syngeneic model to test the TAT allowed for the generation of data on both the early and long-term responses of the microenvironment, particularly regarding immune responses. By optimising the radionuclide-vector-target association, we were able to significantly reduce the amount of vector and activity needed for robust therapeutic efficacy. This places mAbs back at the forefront of potential TAT strategies and validates SDC1 as a relevant GB target.

Reflecting on the initiative of Cordier et al. who investigated TAT as a first intention treatment,[17] and the clinical trial of Zalutsky et al. underscoring the feasibility and minimal toxicity of locoregional ^{211}At administration,[16] forthcoming studies should explore the potential of a TAT using a humanised SDC1 antibody. This direction promises a clinical adaptation of our strategy to address both established tumours and post-operative residual cells. In future perspectives, the brief half-life of ^{211}At also seems compatible with CED implant systems, facilitating treatment delivery without additional surgical procedures.

Contributors

In vivo experiments: LR, SM-L, CR. Mice weighing, sampling and MRI follow-up: LR, SM-L. Antibodies radiolabelling: FG, RE. Cell culture for tumour grafts: LR, SA. Autoradiography: LR, SG. Dosimetry study: NC. Flow cytometry, brain sampling, cryosections and immunofluorescence staining: LR. Data analysis of flow cytometry assays: LR, MA. Histological analysis supervision and interpretation: AR. Statistical analysis: LR, JR. Data verification: LR, JR, EG, MC. Study supervision: EG, MC, FH. Original draft: LR. Writing contribution: EG, MC, FH, RE. All authors reviewed and edited the manuscript before final version. All authors have read and approved the final published version of the manuscript.

Data sharing statement

Comprehensive data are contained within the Article and Supplementary Data. Requests for additional information should be directed to Emmanuel Garcion (emmanuel.garcion@univ-angers.fr) and Michel Chérel (michel.cherel@univ-nantes.fr). The data corresponding to Fig. 1a can be accessed at http://gliovis.bioinfo.cnio.es.

Declaration of interests

The authors declare no competing interest.

Acknowledgements

This work was funded by the French National Agency for Research (ANR) "France 2030 Investment Plan" Labex Iron [ANR-11-LABX-18-01], The SIRIC ILIAD [INCa-DGOS-INSERM-18011], the French program "Infrastructure d'Avenir en Biologie-Santé" (France Life Imaging) [ANR-11-INBS-0006], the PIA3 of the ANR, integrated to the "France 2030 Investment Plan" [ANR-21-RHUS-0012], and support from Inviscan SAS (Strasbourg, France). This work was also funded by the Institut National de la Santé et de la Recherche Médicale (INSERM), the University of Nantes, and the University of Angers. It was also related to: the ANR under the frame of EuroNanoMed III (project GLIOSILK) [ANR-19-ENM3-0003-01]; the "Région Pays-de-la-Loire" under the frame of the Target'In project (to MC and EG); the "Ligue Nationale contre le Cancer" and the "Comité Départemental de Maine-et-Loire de la Ligue contre le Cancer" (CD49) under the frame of the FusTarG project (to EG and AR) and the "Tumour targeting, imaging and radio-therapies network" of the "Cancéropôle Grand-Ouest" (France). LR was a PhD fellow from the LabEx Iron and the University of Angers. We thank the Arronax cyclotron (Saint-Herblain, France) and the IRS-UN technical platforms (SFR François Bonamy, University of Nantes, France) for their support: the CIMA platform, the radioactivity technical platform, the UTE animal facility, the MicroPICell platform, and the Cytocell platform. We also thank the SCAHU animal facility, the Department of Cellular and Tissue Pathology (CHU Angers, France), the PACEM and PRIMEX platforms (SFR ICAT, University of Angers, France), the PRISM core facility (Biogenouest, University of Rennes, University of Angers, INRAE, CNRS, France) and the PRIMEX platform (SFR ICAT, University of Angers, France). We thank Corinne Griguer and G. Yancey Gillespie of the University of Alabama (Birmingham, AL, USA) who provided the GL261 cell line. We thank Marine Dion for her technical

assistance and Marie-Hélène Gaugler for her critical review of the manuscript.

Appendix A. Supplementary data

Supplementary data related to this article can be found at https://doi.org/10.1016/j.ebiom.2024.105202.

References

1 Louis DN, Perry A, Wesseling P, et al. The 2021 WHO classification of tumors of the central nervous system: a summary. *Neuro Oncol*. 2021;23:1231–1251.
2 Ostrom QT, Price M, Neff C, et al. CBTRUS statistical report: primary brain and other central nervous system tumors diagnosed in the United States in 2016-2020. *Neuro Oncol*. 2023;25:iv1–iv99.
3 Stupp R, Mason WP, van den Bent MJ, et al. Radiotherapy plus concomitant and adjuvant temozolomide for glioblastoma. *N Engl J Med*. 2005;352:987–996.
4 Wu Y, Song Y, Wang R, Wang T. Molecular mechanisms of tumor resistance to radiotherapy. *Mol Cancer*. 2023;22(1):96.
5 Taylor MA, Das BC, Ray SK. Targeting autophagy for combating chemoresistance and radioresistance in glioblastoma. *Apoptosis*. 2018;23:563–575.
6 Wu D, Chen Q, Chen X, Han F, Chen Z, Wang Y. The blood–brain barrier: structure, regulation, and drug delivery. *Signal Transduct Targeted Ther*. 2023;8(1):217.
7 Mandel JJ, Yust-Katz S, Patel AJ, et al. Inability of positive phase II clinical trials of investigational treatments to subsequently predict positive phase III clinical trials in glioblastoma. *Neuro Oncol*. 2018;20:113–122.
8 Vanpouille-Box C, Lacoeuille F, Belloche C, et al. Tumor eradication in rat glioma and bypass of immunosuppressive barriers using internal radiation with (188)Re-lipid nanocapsules. *Biomaterials*. 2011;32:6781–6790.
9 Cikankowitz A, Clavreul A, Tétaud C, et al. Characterization of the distribution, retention, and efficacy of internal radiation of 188Re-lipid nanocapsules in an immunocompromised human glioblastoma model. *J Neuro Oncol*. 2017;131:49–58.
10 Séhédic D, Chourpa I, Tétaud C, et al. Locoregional confinement and major clinical benefit of 188Re-loaded CXCR4-targeted nanocarriers in an orthotopic human to mouse model of glioblastoma. *Theranostics*. 2017;7:4517–4536.
11 Eychenne R, Chérel M, Haddad F, Guérard F, Gestin J-F. Overview of the most promising radionuclides for targeted alpha therapy: the 'hopeful eight'. *Pharmaceutics*. 2021;13:906.
12 Wulbrand C, Seidl C, Gaertner FC, et al. Alpha-particle emitting 213Bi-anti-EGFR immunoconjugates eradicate tumor cells independent of oxygenation. *PLoS One*. 2013;8:e64730.
13 Zalutsky MR, McLendon RE, Garg PK, Archer GE, Schuster JM, Bigner DD. Radioimmunotherapy of neoplastic meningitis in rats using an alpha-particle-emitting immunoconjugate. *Cancer Res*. 1994;54:4719–4725.
14 Bäck T, Chouin N, Lindegren S, et al. Cure of human ovarian carcinoma solid xenografts by fractionated α-radioimmunotherapy with 211At-MX35-F(ab')2: influence of absorbed tumor dose and effect on long-term survival. *J Nucl Med*. 2017;58:598–604.
15 Puttemans J, Dekempeneer Y, Eersels JL, et al. Preclinical targeted α- and β–radionuclide therapy in HER2-positive brain metastasis using camelid single-domain antibodies. *Cancers (Basel)*. 2020;12:1017.
16 Zalutsky MR, Reardon DA, Akabani G, et al. Clinical experience with alpha-particle emitting 211At: treatment of recurrent brain tumor patients with 211At-labeled chimeric antitenascin monoclonal antibody 81C6. *J Nucl Med*. 2008;49:30–38.
17 Cordier D, Forrer F, Bruchertseifer F, et al. Targeted alpha-radionuclide therapy of functionally critically located gliomas with 213Bi-DOTA-[Thi8,Met(O2)11]-substance P: a pilot trial. *Eur J Nucl Med Mol Imaging*. 2010;37:1335–1344.
18 Królicki L, Bruchertseifer F, Kunikowska J, et al. Safety and efficacy of targeted alpha therapy with 213Bi-DOTA-substance P in recurrent glioblastoma. *Eur J Nucl Med Mol Imaging*. 2019;46:614–622.
19 Królicki L, Bruchertseifer F, Kunikowska J, et al. Dose escalation study of targeted alpha therapy with [225Ac]Ac-DOTA-substance P in recurrence glioblastoma - safety and efficacy. *Eur J Nucl Med Mol Imaging*. 2021;48:3595–3605.
20 Feng Y, Zalutsky MR. Production, purification and availability of 211At: near term steps towards global access. *Nucl Med Biol*. 2021;100–101:12–23.
21 Guérard F, Maingueneau C, Liu L, et al. Advances in the chemistry of astatine and implications for the development of radiopharmaceuticals. *Acc Chem Res*. 2021;54:3264–3275.
22 Borrmann N, Friedrich S, Schwabe K, et al. Systemic treatment with 4-211Atphenylalanine enhances survival of rats with intracranial glioblastoma. *Nuklearmedizin*. 2013;52:212–221.
23 Watabe T, Kaneda-Nakashima K, Shirakami Y, et al. Targeted alpha therapy using astatine (211At)-labeled phenylalanine: a preclinical study in glioma bearing mice. *Oncotarget*. 2020;11:1388–1398.
24 Liu W, Ma H, Liang R, et al. Targeted alpha therapy of glioma using 211At-labeled heterodimeric peptide targeting both VEGFR and integrins. *Mol Pharm*. 2022;19:3206–3216.
25 Dabagian H, Taghvaee T, Martorano P, et al. PARP targeted alpha-particle therapy enhances response to PD-1 immune-checkpoint blockade in a syngeneic mouse model of glioblastoma. *ACS Pharmacol Transl Sci*. 2021;4:344–351.
26 Kato H, Huang X, Kadonaga Y, et al. Intratumoral administration of astatine-211-labeled gold nanoparticle for alpha therapy. *J Nanobiotechnology*. 2021;19:1–12.
27 Liu Y, Zhou Z, Feng Y, et al. Gold nanostars: a novel platform for developing211at-labeled agents for targeted alpha-particle therapy. *Int J Nanomedicine*. 2021;16:7297–7305.
28 Ma H, Li F, Shen G, et al. In vitro and in vivo evaluation of 211At-labeled fibroblast activation protein inhibitor for glioma treatment. *Bioorg Med Chem*. 2022;55:116600.
29 Gouard S, Maurel C, Marionneau-Lambot S, et al. Targeted-Alpha-therapy combining astatine-211 and anti-cd138 antibody in A preclinical syngeneic mouse model of multiple myeloma minimal residual disease. *Cancers (Basel)*. 2020;12:1–18.
30 Gondelaud F, Ricard-Blum S. Structures and interactions of syndecans. *FEBS J*. 2019;286:2994–3007.
31 Shi S, Zhong D, Xiao Y, et al. Syndecan-1 knockdown inhibits glioma cell proliferation and invasion by deregulating a c-src/FAK-associated signaling pathway. *Oncotarget*. 2017;8:40922–40934.
32 Zhong J, Shi S, Peng W, et al. Weighted gene Co-expression network analysis (WGCNA) reveals the functions of syndecan-1 to regulate immune infiltration by influenced T cells in glioma. *Front Genet*. 2022;13:792443.
33 Zeng L, Zheng W, Liu X, et al. SDC1-TGM2-FLOT1-BHMT complex determines radiosensitivity of glioblastoma by influencing the fusion of autophagosomes with lysosomes. *Theranostics*. 2023;13:3725–3743.
34 Lindegren S, Bäck T, Jensen HJ. Dry-distillation of astatine-211 from irradiated bismuth targets: a time-saving procedure with high recovery yields. *Appl Radiat Isot*. 2001;55:157–160.
35 Guérard F, Navarro L, Lee YS, et al. Bifunctional aryliodonium salts for highly efficient radioiodination and astatination of antibodies. *Bioorg Med Chem*. 2017;25:5975–5980.
36 Hunt Bobo R, Laske DW, Akbasak A, Morrison PF, Dedrick RL, Oldfield EH. Convection-enhanced delivery of macromolecules in the brain. *Proc Natl Acad Sci U S A*. 1994;91:2076–2080.
37 D'Amico RS, Aghi MK, Vogelbaum MA, Bruce JN. Convection-enhanced drug delivery for glioblastoma: a review. *J Neuro Oncol*. 2021;151:415–427.
38 Bolch WE, Eckerman KF, Sgouros G, et al. MIRD pamphlet No. 21: a generalized schema for radiopharmaceutical dosimetry—standardization of nomenclature. *J Nucl Med*. 2009;50:477–484.
39 Ogawa K, Takeda T, Mishiro K, et al. Radiotheranostics coupled between an At-211-Labeled RGD peptide and the corresponding radioiodine-labeled RGD peptide. *ACS Omega*. 2019;4:4584–4591.
40 McLendon RE, Archer GE, Larsen RH, Akabani G, Bigner DD, Zalutsky MR. Radiotoxicity of systemically administered 211At-labeled human/mouse chimeric monoclonal antibody: a long-term survival study with histologic analysis. *Int J Radiat Oncol Biol Phys*. 1999;45:491–499.
41 Le Reste PJ, Pineau R, Voutetakis K, et al. Local intracerebral inhibition of IRE1 by MKC8866 sensitizes glioblastoma to irradiation/chemotherapy in vivo. *Cancer Lett*. 2020;494:73–83.
42 Henry-Stanley MJ, Hess DJ, Erlandsen SL, Wells CL. Ability of the heparan sulfate proteoglycan syndecan-1 to participate in bacterial translocation across the intestinal epithelial barrier. *Shock*. 2005;24:571–576.
43 Reszegi A, Tátrai P, Regs E, Kovalszky I, Baghy K. Syndecan-1 in liver pathophysiology. *Am J Physiol Cell Physiol*. 2022;323:C289–C294.

44 O'Connell FP, Pinkus JL, Pinkus GS. CD138 (Syndecan-1), a plasma cell marker: immunohistochemical profile in hematopoietic and non-hematopoietic neoplasms. *Am J Clin Pathol*. 2004;121:254–263.
45 Green DJ, Shadman M, Jones JC, et al. Astatine-211 conjugated to an anti-CD20 monoclonal antibody eradicates disseminated B-cell lymphoma in a mouse model. *Blood*. 2015;125:2111–2119.
46 Liu YX, Liu WJ, Zhang HR, Zhang ZW. Delivery of bevacizumab by intracranial injection: assessment in glioma model. *OncoTargets Ther*. 2018;11:2673–2683.
47 Resende FFB, Bai X, Del Bel EA, Kirchhoff F, Scheller A, Titze-de-Almeida R. Evaluation of TgH(CX3CR1-EGFP) mice implanted with mCherry-GL261 cells as an in vivo model for morphometrical analysis of glioma-microglia interaction. *BMC Cancer*. 2016;16:1–13.
48 Li Y, Zhang ZX, Huang GH, et al. A systematic review of multifocal and multicentric glioblastoma. *J Clin Neurosci*. 2021;83:71–76.
49 Li S, Dong L, Pan Z, Yang G. Targeting the neural stem cells in subventricular zone for the treatment of glioblastoma: an update from preclinical evidence to clinical interventions. *Stem Cell Res Ther*. 2023;14:1–11.
50 Zhang X, Wu C, Song J, Götte M, Sorokin L. Syndecan-1, a cell surface proteoglycan, negatively regulates initial leukocyte recruitment to the brain across the choroid plexus in murine experimental autoimmune encephalomyelitis. *J Immunol*. 2013;191:4551–4561.
51 Mouthon M-A, Morizur L, Dutour L, Pineau D, Kortulewski T, Boussin FD. Syndecan-1 stimulates adult neurogenesis in the mouse ventricular-subventricular zone after injury. *iScience*. 2020;23:101784.
52 Watanabe A, Mabuchi T, Satoh E, et al. Expression of syndecans, a heparan sulfate proteoglycan, in malignant gliomas: participation of nuclear factor-kappaB in upregulation of syndecan-1 expression. *J Neuro Oncol*. 2006;77:25–32.
53 Wade A, Robinson AE, Engler JR, Petritsch C, James CD, Phillips JJ. Proteoglycans and their roles in brain cancer. *FEBS J*. 2013;280:2399–2417.
54 Couchman JR. Syndecan-1 (CD138), carcinomas and EMT. *Int J Mol Sci*. 2021;22:4227.
55 Gorin JB, Ménager J, Gouard S, et al. Antitumor immunity induced after α irradiation. *Neoplasia*. 2014;16:319–328.
56 Perrin J, Capitao M, Allard M, et al. Targeted alpha particle therapy remodels the tumor microenvironment and improves efficacy of immunotherapy. *Int J Radiat Oncol Biol Phys*. 2022;112:790–801.
57 Lejeune P, Cruciani V, Berg-Larsen A, et al. Immunostimulatory effects of targeted thorium-227 conjugates as single agent and in combination with anti-PD-L1 therapy. *J Immunother Cancer*. 2021;9:e002387.
58 Kim JW, Shin MS, Kang Y, Kang I, Petrylak DP. Immune analysis of radium-223 in patients with metastatic prostate cancer. *Clin Genitourin Cancer*. 2018;16:e469–e476.
59 Bellia SR, Feliciani G, Del Duca M, et al. Clinical evidence of abscopal effect in cutaneous squamous cell carcinoma treated with diffusing alpha emitters radiation therapy: a case report. *J Contemp Brachytherapy*. 2019;11:449–457.
60 Behling K, Maguire WF, Di Gialleonardo V, et al. Remodeling the vascular microenvironment of glioblastoma with α-particles. *J Nucl Med*. 2016;57:1771–1777.
61 Jameson SC, Masopust D. Understanding subset diversity in T cell memory. *Immunity*. 2018;48:214–226.
62 Genoud V, Marinari E, Nikolaev SI, et al. Responsiveness to anti-PD-1 and anti-CTLA-4 immune checkpoint blockade in SB28 and GL261 mouse glioma models. *Oncoimmunology*. 2018;7:e1501137.
63 Zhang J, Li F, Yin Y, et al. Alpha radionuclide-chelated radioimmunotherapy promoters enable local radiotherapy/chemodynamic therapy to discourage cancer progression. *Biomater Res*. 2022;26:1–15.
64 Brown CE, Alizadeh D, Starr R, et al. Regression of glioblastoma after chimeric antigen receptor T-cell therapy. *N Engl J Med*. 2016;375:2561–2569.
65 Liau LM, Ashkan K, Brem S, et al. Association of autologous tumor lysate-loaded dendritic cell vaccination with extension of survival among patients with newly diagnosed and recurrent glioblastoma: a phase 3 prospective externally controlled cohort trial. *JAMA Oncol*. 2023;9:112–121.
66 Obata H, Ogawa M, Zalutsky MR. DNA repair inhibitors: potential targets and partners for targeted radionuclide therapy. *Pharmaceutics*. 2023;15:1926.
67 van Solinge TS, Nieland L, Chiocca EA, Broekman MLD. Advances in local therapy for glioblastoma — taking the fight to the tumour. *Nat Rev Neurol*. 2022;18:221–236.
68 Zhang J, Qin S, Yang M, Zhang X, Zhang S, Yu F. Alpha-emitters and targeted alpha therapy in cancer treatment. *iRADIOLOGY*. 2023;1:245–261.